Jagiellonian University
Faculty of Physics, Astronomy and Applied Computer Science

Assembly and calibration of apparatus for Positron Annihilation Lifetime Spectroscopy

Master thesis
Advanced Materials and Nanotechnology

Author
Kamil Dulski

Supervisor
Prof. dr hab. Paweł Moskal
Department of Nuclear Physics

Kraków 2016

Contents

Oświadczenie autora pracy

Świadom odpowiedzialności prawnej oświadczam, że niniejsza praca dyplomowa została napisana przeze mnie samodzielnie i nie zawiera treści uzyskanych w sposób niezgodny z obowiązującymi przepisami.

Oświadczam również, że przedstawiona praca nie była wcześniej przedmiotem procedur związanych z uzyskaniem tytułu zawodowego w wyższej uczelni.

Kraków, dnia Podpis autora pracy

Oświadczenie kierującego pracą

Potwierdzam, że niniejsza praca została przygotowana pod moim kierunkiem i kwalifikuje się do przedstawienia jej w postępowaniu o nadanie tytułu zawodowego.

Kraków, dnia Podpis kierującego pracą

Acknowledgments

I would like to thank all people without whom this thesis would not be created

Firstly, I would like to express my deep gratitude to Prof. Paweł Moskal for his endless patience, guidance and enormous help writing this thesis. Furthermore, from Prof. Paweł Moskal I could always expect an excellent solution to problems appearing during measurements and analysis.

I thank my colleagues Ewelina Kubicz and Anna Wieczorek for help in the first moments in group and for a lot of interesting and valuable conversations. They always were ready to help me with every issues that appeared in laboratory.

I wish to thank also Dr Bartosz Głowacz and Dr Marcin Zieliński for their suggestions and remarks during group mettings.

Abstract

Positron Annihilation Lifetime Spectroscopy (PALS) apparatus was assembled using two BaF_2 detectors, and oscilloscope. Assembled setup then was optimized, by finding the best settings and parameters to collect large number of events, used in further analysis. Sodium isotope ^{22}Na was used as source of positrons. A constructed setup measured time difference distribution between acts of positron emission and its annihilation (positron lifetime in the studied material). A computer procedure developed in the framework of this thesis enabled to analyze measured spectra and to extract average lifetimes distributions including contribution from direct annihilation as well as from the annihilation from para- and ortho-positronium atoms. Two samples, silicon plates (Si) and polyvinyl toluene (PVT) were measured. Results from analysis showed that, these two samples differ significantly in distribution of lifetime, as one of them is porous (PVT) with pore sizes of around 0.277 and 0.356 nm, while other is crystalline. Moreover, a new research proposal was described aiming at the investigations of SAMs(Self Assembled Monolayers) and low-κ dielectrics.

Abstrakt

Układ do pomiarów Spektroskopii Czasów Życia Pozytonów (Positron Annihilation Lifetime Spectroscopy - PALS) został złożony z dwóch detektorów BaF_2 i oscyloskopu. Układ został następnie zoptymalizowany, poprzez znalezienie najlepszych parametrów pracy detektora i ustawień oscyloskopu, zbierając jak najwięcej zdarzeń, używanych przy dalszej analizie czasów życia. Izotop ^{22}Na został użyty jako źródło pozytonów. Zestawiony układ mierzył rozkład różnic czasów między aktami emisji pozytonu i jego annilhilacji (czas życia pozytonu w badanym materiale). Procedura komputerowa rozwinięta w ramach tej pracy pozwoliła do zanalizowania zebrane widma i uzyskania z nich rozkładów średnich czasów życia, zawierających zarówno wkład od bezpośredniej anihilacji pozytonów jak i wkład od annihilacji para- i orto-pozytonium . Dwie próbki, płytki krzemowe (Si) i poliwinylotoluen (PVT) zostały zmierzone. Wyniki pokazały, że te dwie próbki różniły się znacząco pod kątem rozkładu czasów życia. Zaobserwowano, że jedna próbka była porowata z porami o średnicy około 0.277 i 0.356 nm, podczas gdy druga była krystaliczna. Ponadto opisano propozycję dalszych badań samo organizujących się warstw(z ang. SAM) i dielektryków z niską wartością stałej dielektrycznej (z ang. low-κ dielectrics).

Chapter 1

Introduction

1.1 Motivation

Motivation of this thesis is to get knowledge about Positron Annihilation Lifetime Spectroscopy (PALS) measurements and to elaborate methods for collecting and analysis of data from measurement. This knowledge will be useful for elaboration of the PALS experimentation with the Jagiellonian-PET (J-PET) detector. Idea of J-PET detector is described in [1] - [8]. Activating PALS in such tomograph, will bring new possibilities in medical imaging and in scientific research [9]-[11].

PALS technique itself is great tool for characterizing nanomaterials, as it is sensitive to the size of pores or free volumes in the order of nanometers like in zeolites or MOF(Metal Organic Framework). Thanks to the possibility of structural characterization of the material, PALS enable to study microstructural phase transitions or degeneration degree [12]. With controlled deposition of positrons depth, one can get information about arrangement of layers in material [13]. This could be helpful in quality control of new types of nanomaterials, used for example in organic solar cells.

1.2 Positron Annihilation Lifetime Spectroscopy (PALS)

Positron Annihilation Lifetime Spectroscopy is a non-destructive research technique, which is based on lifetime of ortho-positronium dependency on the free volume radius. Free volume is a term, created to characterize volume in material, wherein electron density equals to zero. Exemplary scheme of free volume is shown in Fig. 1.1. In zeolites free volumes can be interpreted as channels, where molecules can diffuse through material.

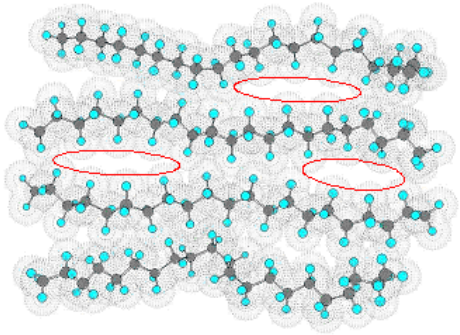

Fig. 1.1. Free Volumes between polymer chains, marked as red ellipses. The Figure is adapted from [14].

Positronium is an atom-like state of electron and positron. Positron is an antiparticle to electron, and it is created for example through β^+ decay of ^{22}Na as indicated in Fig. 1.2. Positron has the same properties as electron, and differs from electron only in sign of its electric charge.

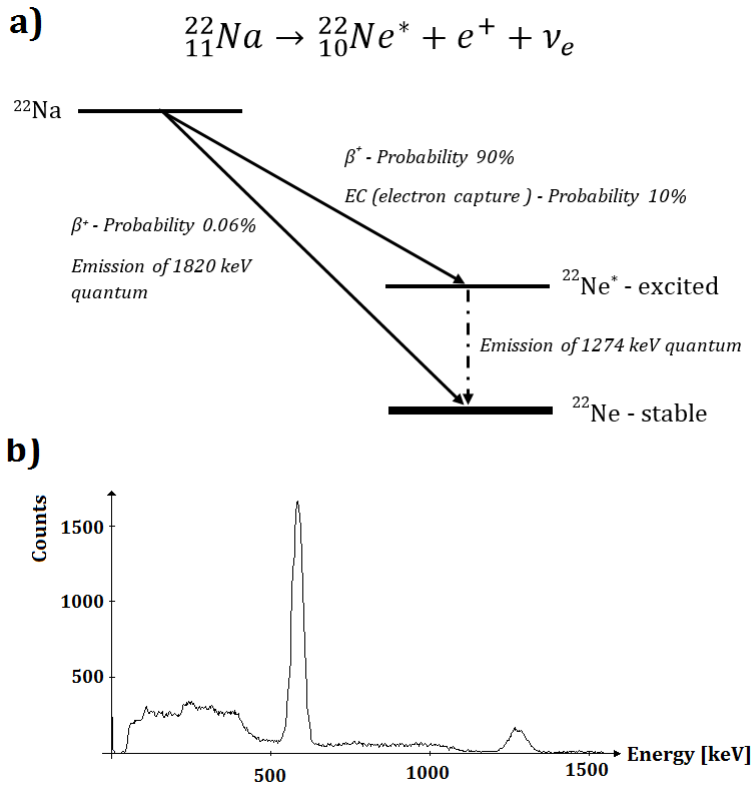

Fig. 1.2. (a) Scheme of β^+ decay of ^{22}Na isotope (b) Energetic spectrum induced by gamma quanta originating from the ^{22}Ne decay and subsequent e^+e^- annihilation. The Figure is adapted from[15].

When positron is deposited into material, its kinetic energy is lost through ionization and excitation of material molecules. After thermalisation positron annihilates directly with electron or via creation of positronium as shown in Fig. 1.3a. Positronium itself can exist in

two states, depending on total spin of it. Para-positronium (p-PS) is formed when positronium total spin is equal to zero. If the total spin is equal to one, ortho-positronium (o-Ps) is created. Difference between these two states is in the way they decay. Para-positronium decays very quickly (average decay time is around 0.125 ns) with emission of even number of gamma quanta. Usually it decays with emission of two gamma quanta, with the same energy 511 keV (electron/positron rest energy) in the same direction but with opposite sense. Ortho-positronium decay time is longer (average decay time is around 142 ns), with emission of odd number of gamma quanta, greater or equal than 3. The whole process is shown in Fig. 1.3b.

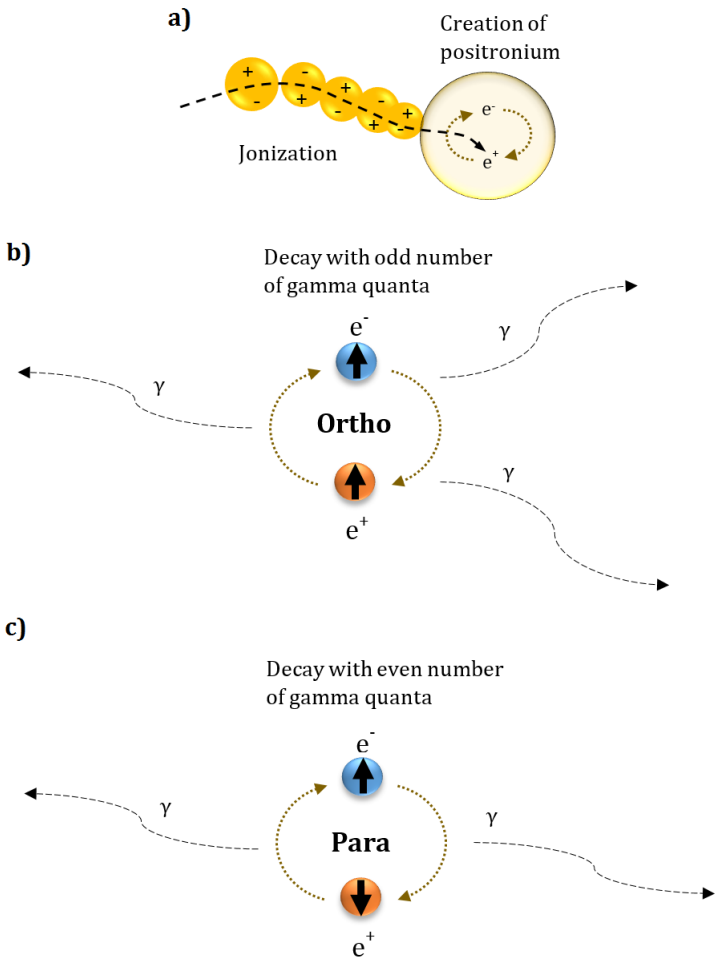

Fig. 1.3. (a) Scheme of creation of positronium after depositing positron to material. (b) Scheme of ortho-positronium and its decay. c) Scheme of para-positronium and its decay.

In PALS, average lifetime of the created positronium is estimated, as the time difference between deexcitation and annihilation event in material.

1.3 Use of PALS for characterizing the materials

In condensed matter ortho-positronium will decay with average lifetime shorter than in vacuum (142 ns). This happens usually due to pick-off process. This process is based on uptake of electron from surroundings, and switching it with the electron from positronium atom. Uptaken electron and positron can create para-positronium, which decays with its mean lifetime of 0.125 ns. The whole process is shown in Fig. 1.4.

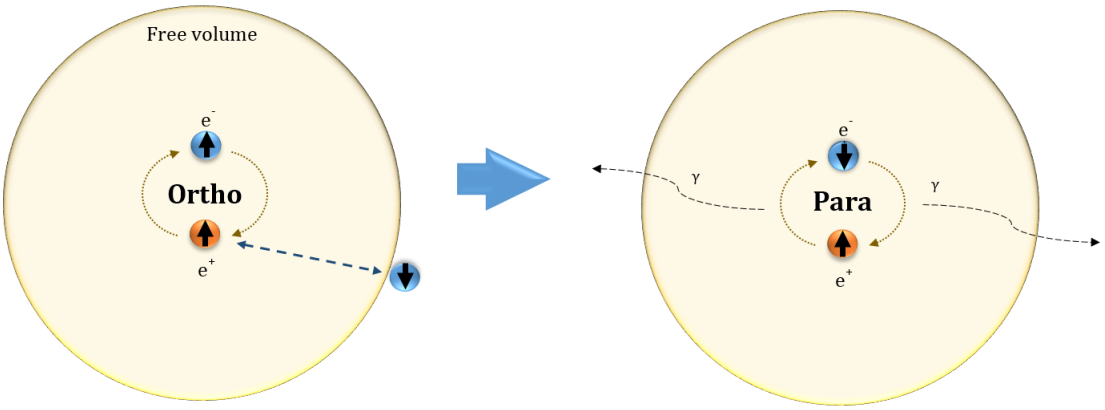

Fig. 1.4. Scheme of pick-off process.

Pick-off process shortens mean lifetime of positronium. Probability of this process decreases with increase of the size of free volume, because it is more unlikely that positron from ortho-positronium will uptake electron from surroundings. This dependency is useful for characterizing materials, because shortening of positronium mean lifetime is strongly correlated with free volume sizes in material.

The most popular equation connecting average lifetime of ortho-positronium and free volume size is given by Tao-Eldrup formula:

$$\tau_{Ps} = \frac{1}{2}\left(1 - \frac{R}{R+R_0} + \frac{1}{2\pi}\sin\left(\frac{2\cdot\pi\cdot R}{R+R_0}\right)\right)^{-1}, \tag{1.1}$$

Tao-Eldrup model applies to the spherical free volumes with radius between 1 nm to around 6 nm [16], however it gives quite accurate results down to 0.1 nm. τ_{Ps} is the average lifetime of positronium, R denotes the radius of free volume and R_0 empirical value equal to 0.166 nm [16].

Using lifetime dependence of free volume radius, one can calculate diameter of pores in condensed material, which could characterize diffuse properties of material. It is particularly important in zeolites or other molecular sieves, where size of the channel in material determines size of molecules which can diffuse through it. What is important, PALS is non-destructive and more precise than commonly used techniques based on adsorption isotherm [17].

1.4 Proposal of future studies with PALS

This thesis is a first step on a way to perform a feasibility study of application of PALS to measurements of structure of self assembled monolayer (SAM). SAMs is the aliphatic chains, which has property to assembly in layer on surfaces, without any outside interference. They assembly due to minimization of the van der Waals interactions between each aliphatic chain. Exemplary process of creating SAM, used in measurements, is shown in Fig. 1.5.

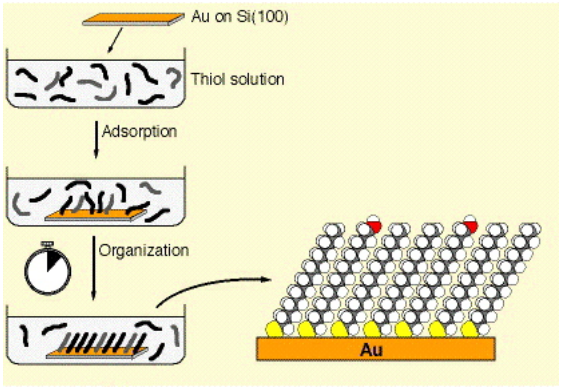

Fig. 1.5. Exemplary scheme of obtaining SAM. The Figure is adapted from[18].

Self assembly molecules chains need some time in solution, to organize on surface. PALS measurements will provide information how average lifetime of ortho-positronium changes as a function of time in solution of substrate. Average lifetime of ortho-positronium should decrease in time as the degree of crystallinity increases [[19], Figure 3]. Subsequently, the average lifetime of o-Ps should not change anymore in time after the organization of molecules in the layers is finalized. That property bring possibility to determine optimal duration of obtaining SAM, useful for further synthesis of this type of molecules.

In substrate which is usually metal or semi-conductor, which is densely packed and with high electron density in whole material, there is very unlikely that ortho-positronium will be created, so in measurements one should see only signal from self assembled monolayer.

The above outlined proposition of studies could be transferred into another class of nanomaterials. Low κ dielectrics have very low value of dielectric constant κ relative to silicon dioxide, what leads to its higher resistance. This kind of materials found application in development of electronics, where size of transistors or other microsystems is being reduced to the limits. For example low κ dielectric can be used instead of silicon dioxide layer in transistors. Higher resistance, with the same size of layer, will provide better insulation from interference during switching between gate and terminal connecting source and drain, what will improve work of transistors with no need to reduce the size of insulation layer.

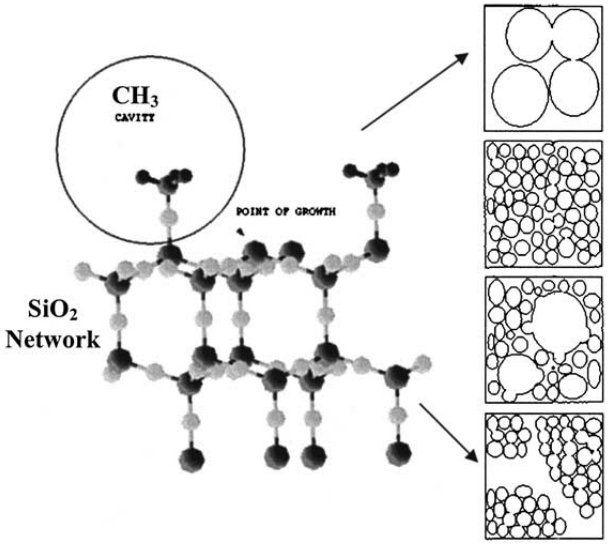

Fig. 1.6. Porosity formation process in low κ dielectrics. The figure is adapted from[20].

Low value of dielectric constant is obtained by inducing bigger pores in dielectric material (for example in SiO_2, Fig. 1.6), which are responsible for bigger value of resistance than in silicon dioxide. Dielectric with low value of κ, could be produced by depositing dielectric material on substrate, for example through chemical vapor deposition [21]. The idea for experiment is similar to previous proposal. The plan is to characterize process of producing low κ dielectric film, through measurements of pores size distribution and resulting resistance of material. Dependence of resistance on radius of pores could be helpful in estimating optimal condition of producing low κ thin films [21].

Chapter 2

Detection system

In this chapter the process of detection system assembling, used configurations and materials will be described. Also a procedure of data analyzing collected with the oscilloscopes and further optimization of the settings will be shown.

2.1 PALS setup configurations used in measurements

PALS setup consisted of two BaF_2 detectors assembled by SCIONIX Holland with Hamamatsu photomultipliers with serial numbers SBO696 and SBO697, CAEN SY4527 high voltage power supply (HV), LeCroy 6000A serial data analyzer oscilloscope (SDA) and ^{22}Na radioactive isotope. Two ^{22}Na sources have been used: one was placed in polymer (37/12, activity around 300 kBq) and the other in the Kapton (activity around 1.3 MBq)[1][11].

In Positron Annihilation Lifetime Spectroscopy measurements, two geometrically different setups are used. These setups differ in the angle between two detectors and position of the source. Both are shown in Fig. 2.1.

Setup with parallel positions of detectors (180^o) was used, because it allows to collect satisfactory number of events both for 511 keV and 1274 keV gamma quanta. The gamma quanta with energy of 511 keV comes from electron-positron annihilation, and 1274 keV comes from deexcitation of Ne. The shift of the source from the detector axis was larger than the radius of the BaF_2 crystals. Such configuration provided that only 511 and 1274 quanta could be registered in coincidence and registration of both 511 quanta was geometrically prohibited.

[1]Sources were produced by Dr B. Zgardzinska and Prof. B. Jasinska at the Maria Curie Sklodowska University in Lublin

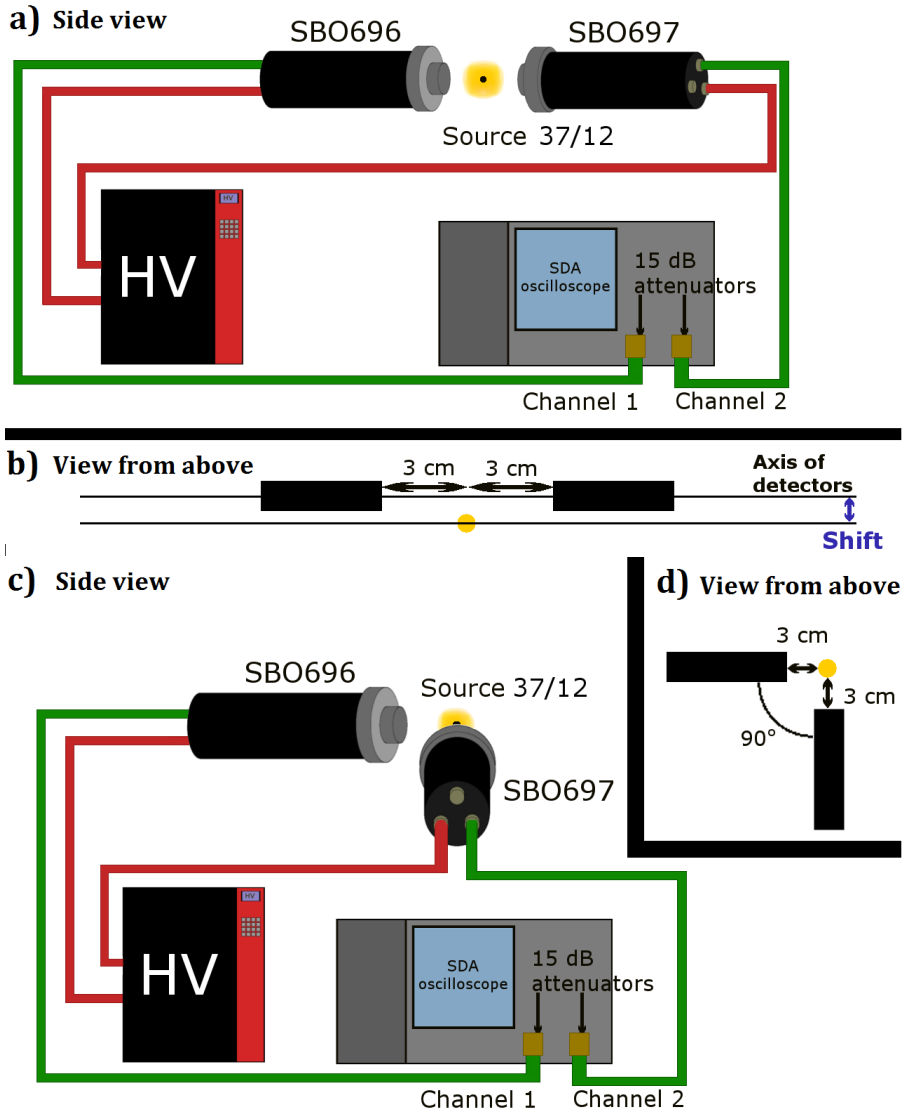

Fig. 2.1. Setup model with angle between detectors equal to 180 ^{o} (a), and its projection (b). Setup model with angle between detectors equal to 90 ^{o} used in calibration measurements (c) and its projection (d).

For the practical purposes, signal cables with different lengths were used. One of the reasons for offset of time difference between two signals coming from the same annihilation. Offset value is due to the difference in length of cables and due to differences of signal generation and propagation in detectors and electronics.

2.2 Method of data analysis

Oscilloscope used in the measurements (Serial Data Analyser - SDA) was collecting signals from two BaF_2 detectors. Signal is the dependency of voltage over time, at given channel of the oscilloscope. Collecting a waveform of single signal allows to calculate its *charge*, *amplitude*, *pedestal*, *rise time* and *time* at given voltage threshold.

When gamma quantum hits the BaF_2 detector, negative signal is produced in detector which then go to oscilloscope. Exemplary signal is shown in Fig. 2.2a.

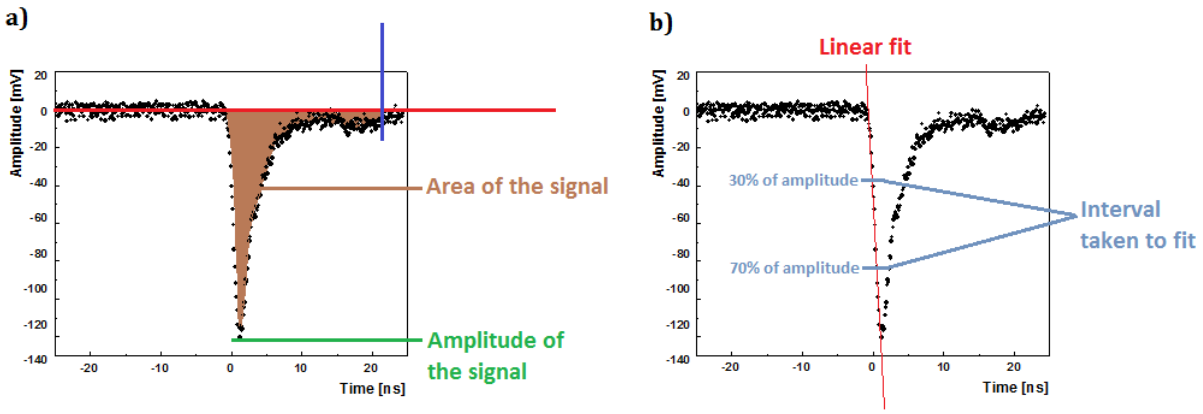

Fig. 2.2. (a) Example of a signal collected by SDA oscilloscope. Vertical blue line indicate a limit used for the determination of the signal area. Pedestal of the signal is denoted with the red horizontal line.
(b) Procedure of linear fitting to the leading edge of the signal used for the time calculation.

The signal pedestal (Ped) is calculated as the mean of the first 20 points of the signal from the left side. It is needed in further calculation of charge, amplitude and times.
Amplitude (Amp) is the minimum of the signal in measured time window.
Signals measured by oscilloscopes are sampled in discrete time points with 50 ps intervals. The time at given voltage threshold is estimated based on the line fit to the leading edge in the range between 30% and 70% of the *Amplitude*, as it is shown in Fig. 2b. Slope is interpolated with the linear fit from the selected points (Eq. (2.1))

$$U(t) = a \cdot t + b \tag{2.1}$$

where a and b are the parameters of the fit, t is time, and U is the signal voltage at given time. Time (t_{Thr}) at given voltage threshold (U_{thr}) at the leading edge is now calculated from Eq. (2.2)

$$t_{Thr} = \frac{U_{thr} - b}{a}. \tag{2.2}$$

Rise time (RT) is defined as the difference of the times at 10% and 90% of the amplitude of the signal :

$$RT = t_{90\%Amp} - t_{10\%Amp}. \tag{2.3}$$

Charge (Q) of the signal may be expressed by relation:

$$Q = \int I(t)dt, \tag{2.4}$$

for the current I, and time t. $I(t)$ may be expressed using Ohm's Law as:

$$I(t) = \frac{U(t)}{R}, \tag{2.5}$$

where U is the electric voltage and R is the resistance. Applying Eq. (2.4) and (2.5) a charge Q can be determined as:

$$Q = \int \frac{U(t)dt}{R}. \tag{2.6}$$

Value of $\int U(t)dt$ is calculated as the area under the signal and R is the resistance of the channel of the oscilloscope. This resistance is constant for all measurements and is equal to 50 Ω.

Calculating area of given signal requires individual approach, due to time window of the oscilloscope, which is not wide enough to measure a whole long decaying component of the signal produced by BaF_2 detectors ($\approx$ 630 ns[2]). Additionally signals from one coincidence are registered at different time with respect to the beginning of the oscilloscope time window. This generates charge dependency on the time of signal registration. In order to avoid this charge variations, the area is calculated only in the range from t_{Ped} till 300 points after t_{Amp} of given signal, where t_{Ped} and t_{Amp} denote the time at the beginning and the time at the amplitude of the signal, respectively. The time t_{Ped} is defined as a time at which a line fitted to the leading edge (Fig. 2.2) crosses the pedestal level. Number 300 was chosen as a constant value for all analyzed signals. Charge is then calculated as the absolute value of area of the signal, subtracted by product of the pedestal (Ped) and range of integration:

$$Q[C] = |\frac{Area_{signal} - Area_{Ped}}{50}|\frac{[Vs]}{[\Omega]}; \qquad Area_{Ped} = Ped \cdot (t_{Amp} + 300 \cdot 50ps - t_{Ped}) .$$

2.3 Setup assembly

First measurements focused on estimation of the maximal amplitude of signals generated by BaF_2 detectors. It was essential in order to use LeCroy SDA scope, as signals greater than $\approx$ 15 V can overcharge inputs of channels and damage the device. To estimate maximal amplitudes Waveform oscilloscope was used, which allows to measure signals with higher amplitudes, but less accurate. Setup contained detectors connected to oscilloscope and high voltage supplier. Measurements were performed with cosmic radiation, and lasted for around 24 hours for each detector. Oscilloscope (with settings shown in Tab. 2.1) gathered histograms of amplitude.

Table 2.1: Settings for overcharge measurement

Trigger level	**Scale**	**Binning**	**Voltage on detector**
-5 V	5 ns / 10 V	200	2500 V

[2]http://www.crystals.saint-gobain.com/uploadedFiles/SG-Crystals/Documents/Barium%20Fluoride%20Data%20Sheet.pdf

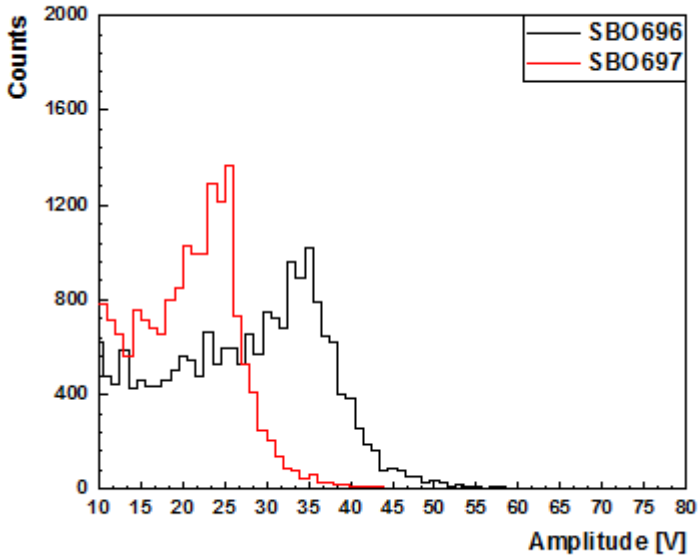

Fig. 2.3. Amplitude distribution of signals from cosmic radiation measured with Waverunner oscilloscope. Settings used in measurement are shown in Tab. 2.1. Results obtained for different detectors are shown with different colors as indicated in the legend.

Results of this measurement for both detectors are shown in Fig. 2.3. Maximal amplitudes had occured around 70 V. As LeCroy SDA can safely accept signals with amplitude lower than 15 V, in further experiments signals were attenuated. Appropriate attenuation value (T) was calculated with formula (2.7):

$$T[dB] = 20 \log_{10} \frac{U_{in}}{U_{out}}, \tag{2.7}$$

where U_{in} is the input electric voltage, and U_{out} the output electric voltage.
In this case signals should be attenuated from 70 V to at most 15 V, therefore minimal attenuation reads:

$$T_{min} = 20 \log_{10} \frac{70}{15} \approx 13.4 \; dB.$$

Therefore, based on the above calculations, for all further measurements 15 dB attenuators were used on the inputs of the oscilloscope. Then, test measurement with the settings shown in Tab 2.2 was performed.

Table 2.2: Settings for measurements with attenuators

Trigger level	**Scale**	**Binning**	**Voltage on detector**
-1 V	5 ns / 2 V	200	2500 V

Results are shown in Fig. 2.4. As one can observe when applying attenuators, maximal amplitudes are around 12 V, enabling a safe use of LeCroy SDA with BaF_2 detectors.

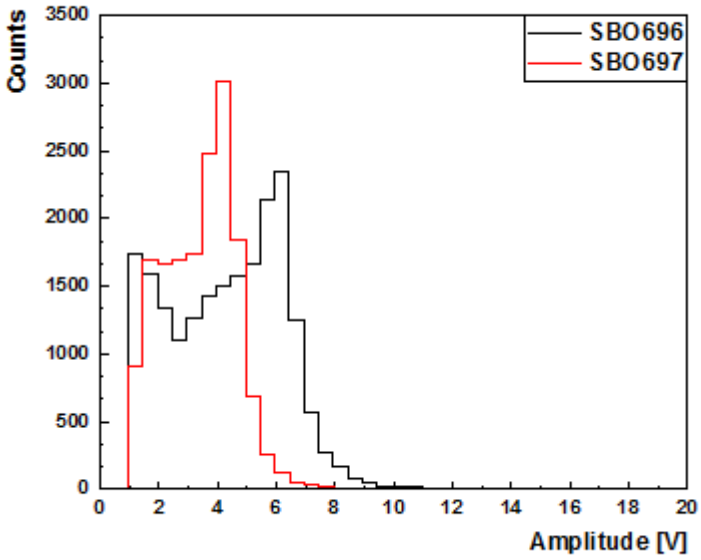

Fig. 2.4. Amplitude distributions of signals from cosmic rays registered with Waverunner oscilloscope with 15 dB attenuators and the supply voltage of 2500 V. Results obtained for different detectors are shown with different colors as indicated in the legend.

2.4 Gain calibration

Setup used for gain calibration is shown in Fig. 2.1a, where the radioactive source ^{22}Na covered with polymer, was shifted by about 2 cm. From the collected signals, charge and amplitude histograms were calculated (Fig. 2.5). Setting used for this measurement are presented in Tab. 2.3.

Table 2.3: Exemplary settings for gain measurement

Settings for both channels						
Trigger	**Coincidence**	**Scale**	**Offset**	**Voltage on detectors**	**Timescale**	**Delay**
-20.1 mV	Channel 2 after Channel 1	30 mV/div	115 mV	2200 V	10 ns/div	10 ns

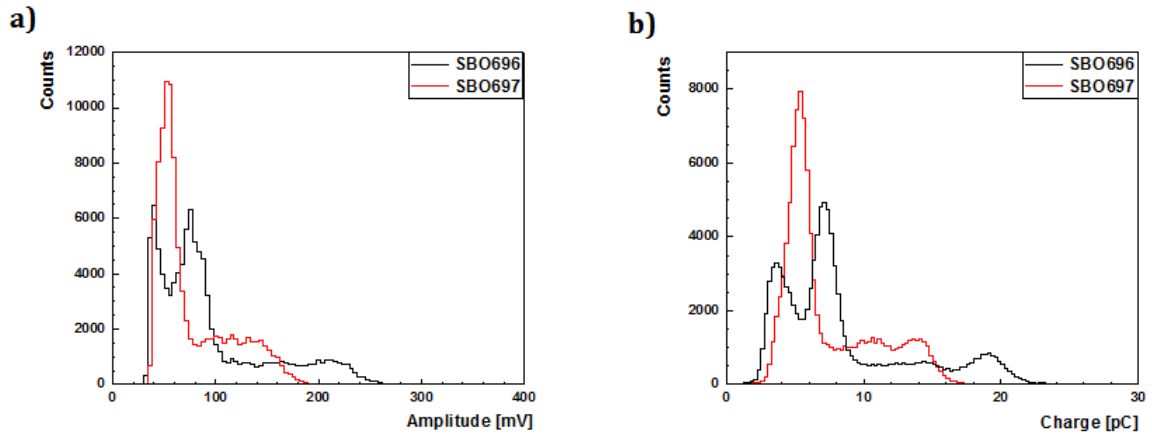

Fig. 2.5. Distribution of amplitude (a) and charge (b) of signals measured with settings as in Tab. 2.3. Results obtained for different detectors are shown with different colors as indicated in the legend.

Charge of the signal is proportional to energy deposited in the detector by the gamma quantum. In Fig. 2.6 energy loss spectrum for ^{22}Na is shown. This spectra can be divided into four parts, each dominated by the different type of signals originating from different types of gamma quanta and physical phenomena of its interaction in scintillators. Two of them come from photoelectric effects in BaF_2 crystal, one caused by annihilation quantum (511 keV) and other by deexcitation quantum (1274 keV). The other two come from Compton scattering in detector material of the aforementioned gamma quanta.

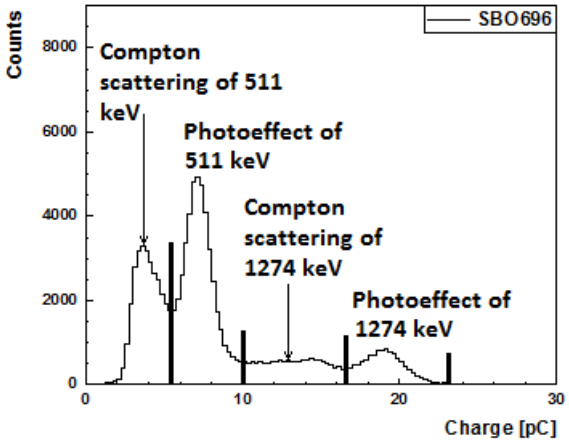

Fig. 2.6. ^{22}Na charge spectrum obtained with BaF_2 scintillator. Vertical lines indicates regions of dominance of various effects described inside the figure.

Due to different gain on each detector one can observe that charge spectra shown in Fig. 2.5 are not matched with each other, as it should be. Gain is the term that characterize how effectively detector strengthens the signal created by registered gamma quantum. Gain is strongly dependent on voltage. In order to determine the dependence of the gain from the applied voltage (HV) a series of measurements were performed for following HV values:

2000, 2100, 2200, 2250, 2300, 2350, 2400, 2425, 2450, 2475, 2500 V.
Settings on oscilloscope was as in Tab. 2.3, except the scale and offset values, which was selected to each supply voltage, in order to see full signals.

In order to model gain dependence on the applied voltage following considerations were done. When photon hits the photomultiplier's (PM) photocathode, it can release a photoelectron. This emitted electron is then accelerated in an electric field, towards next dynode, which hit by electron can release secondary electrons, as shown pictorially in Fig. 2.7. For a given electric field between two dynodes ($U^{(HV)}$), one can use a following expression for average multiplication of number of electrons δ:

$$\delta = A \cdot \left(U^{(HV)}\right)^{\alpha}, \tag{2.8}$$

where A is constant, and α is coefficient based on geometric structure of dynodes.

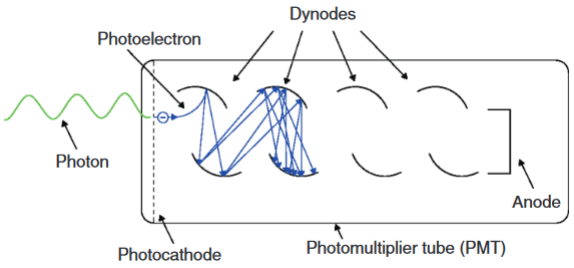

Fig. 2.7. Secondary emission scheme in photomultiplier. Figure is adapted from [[22], *Fig. 1*].

Assuming that in photomultiplier there is n identical dynodes, gain (μ) defined as amplification of single electron can be expressed by:

$$\mu = \delta^n = A^n \cdot \left(U^{(HV)}\right)^{n\cdot\alpha} = K \cdot \left(U^{(HV)}\right)^{n\cdot\alpha}, \tag{2.9}$$

where K is constant. Charge of the signal produced by given amount of light that reached photocatode will be proportional to the gain of the photomultiplier [22].

In further analysis, we use charge at photoelectric maximum for 511 keV gamma quanta (G), as a measure of photomultiplier gain. Figure 2.8 shows G as a function of the voltage $U^{(HV)}$ supplied to the photomultiplier. Based on Eq. (2.9) we assume that G is related with $U^{(HV)}$ as follows:

$$G = a \cdot \left(U^{(HV)}\right)^{b}, \tag{2.10}$$

where a and b are parameters of the fit.

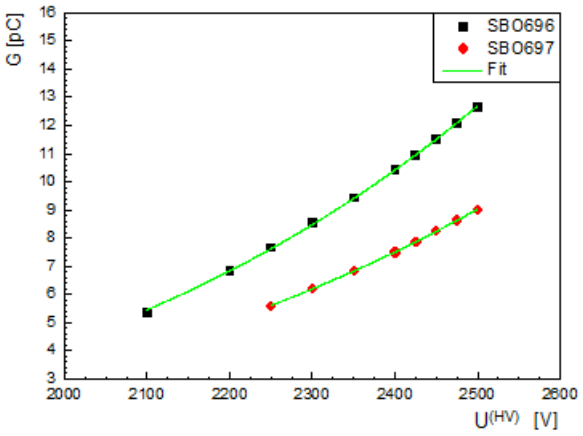

Fig. 2.8. Dependence of G as a function of $U^{(HV)}$. Squares and diamonds denote results of measurements and superimposed lines show result of the fit of formula (2.10) to the data. As a result of the fit it was established that: $a_1 = 4.62(13)\ 10^{-16}\frac{pC}{V}$, $b_1 = 4.838(36)$, $a_2 = 4.41(23)\ 10^{-15}\frac{pC}{V}$, $b_2 = 4.506(21)$

Results from gain calibration measurements with fitted function are shown in Fig. 2.8. Detector with serial number SBO696 had higher gain than SBO697. In order to obtain the same gains for both detectors, a voltage supplied to the SB0697 module was changed. The new value of the voltage was determined solving a following system of equations:

$$\begin{cases} G_1 = a_1 \cdot \left(U_1^{(HV)}\right)^{b_1} \\ G_2 = a_2 \cdot \left(U_2^{(HV)}\right)^{b_2} \\ G_1 = G_2, \end{cases}$$

where G_1 and G_2, and $U_1^{(HV)}$ and $U_2^{(HV)}$ denote gains and voltages applied to detectors SBO696 and SBO697, respectively. Simple calculations allows to determine formula for $U_2^{(HV)}$, as a function of $U_1^{(HV)}$:

$$U_2^{(HV)} = \left(\frac{a_1}{a_2}\left(U_1^{(HV)}\right)^{b_1}\right)^{\frac{1}{b_2}} \tag{2.11}$$

Thus, for example when setting $U_1^{(HV)} = 2300$ and $U_2^{(HV)} = 2465$ V one obtains the same gain at both detectors.

Detector settings used in measurements, after gain calibration is shown in Tab. 2.4 and charge and amplitude spectra after the gain calibration are shown in Fig. 2.9.

Table 2.4: Settings for measurement after gain calibration

Trigger	Coincidence	Scale	Offset	Voltage on detectors	Timescale	Delay
Settings for channel 1						
-42.0 mV	Channel 2 after Channel 1	50 mV/div	192 mV	2300 V	10 ns/div	10 ns
Settings for channel 2						
-36.0 mV	Channel 2 after Channel 1	50 mV/div	192 mV	2465 V	10 ns/div	10 ns

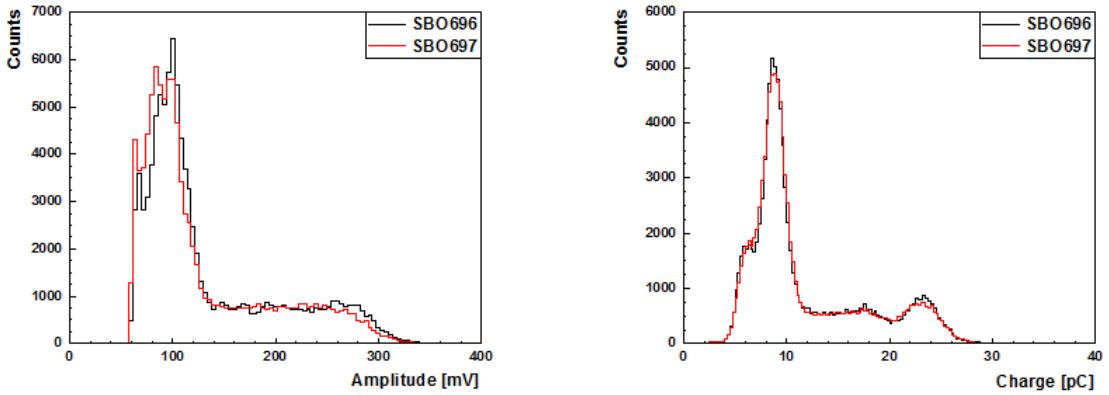

Fig. 2.9. Distribution of amplitude (a) and charge (b) measured with the detectors settings given in Tab. 2.4. Results obtained for different detectors are shown with different colors as indicated in the legend.

2.5 Settings optimization

In PALS measurement, it is important, to collect as much and as fast as possible events when one detector registers gamma quanta coming from deexcitation, and the other quanta from annihilation. Further on we will refer to such events as "1274-511". Thus the best configuration of the setup is when fraction of „1274-511" events is large compared to „511-511" events.

To collect „1274-511" fraction effectively, one can assign one detector to collect only gamma quanta coming from deexcitation, whereas the second one should collect quanta from annihilation. In the experiment discussed in this thesis, it was done by setting on the channel of oscilloscope that was connected to SBO696 a very high trigger level in order to discriminate significant part of the signals from 511 keV quanta, and as a result SBO696 detector collects almost always deexcitation quanta. Settings of the measurement are shown in Tab. 2.5. Registered amplitude and charge spectra are shown in Fig. 2.10.

Table 2.5: Settings with high trigger on one detector

Trigger	Coincidence	Scale	Offset	Voltage on detectors	Timescale	Delay
Settings for channel 1						
-110.0 mV	Channel 2 after Channel 1	50 mV/div	192 mV	2300 V	10 ns/div	10 ns
Settings for channel 2						
-8.0 mV	Channel 2 after Channel 1	20 mV/div	78 mV	2465 V	10 ns/div	10 ns

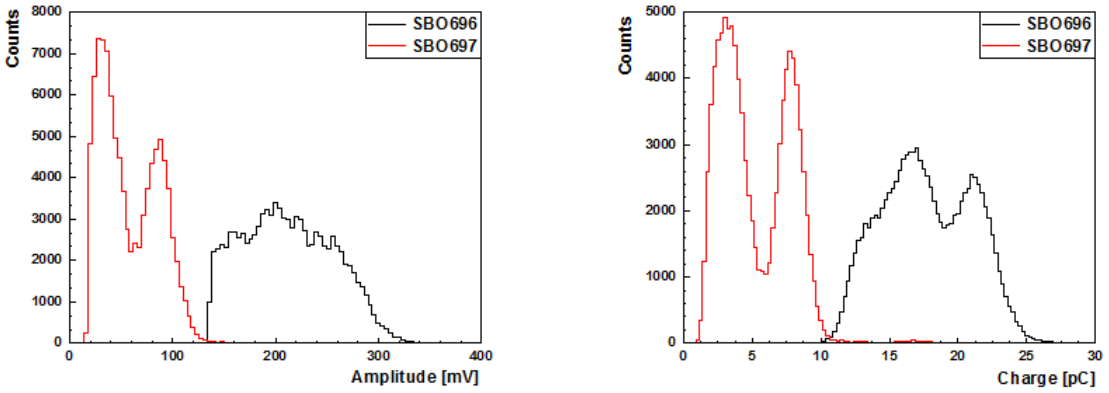

Fig. 2.10. Distribution of amplitude (a) and charge (b) of signals collected with high threshold set at SBO696 detector. Results obtained for different detectors are shown with different colors as indicated in the legend.

2.6 Analysis optimization

In the measurement waveforms of all signals fulfilling triggering conditions were collected. As a next step of analysis a time difference between registration of annihilation and deexcitation quantum will be determined. However due to the noise and due to the time walk effect, the time resolution depends on the value of voltage level (software threshold) at which the time is calculated. In this chapter an optimum values of software thresholds will be determined.

Obtaining the best threshold for events in which 511 keV gamma quanta on both detectors are collected, was first thing to do. The setup was assembled as in Fig. 2.1a, but with source shift equal to zero, and setting as in Tab. 2.6. Two gamma quanta with energy from 511 keV regime should, with very high probability, come from the same annihilation in the material of the source. Time differences between these two signals coming from the same annihilation should be then spread symmetrically around value that comes only from different cable lengths and responses of detectors.

Table 2.6: Settings for first step of analysis optimization

Trigger	Coincidence	Scale	Offset	Voltage on detectors	Timescale	Delay
Settings for channel 1						
-25.0 mV	Channel 2 after Channel 1	50 mV/div	192 mV	2300 V	10 ns/div	10 ns
Settings for channel 2						
-23.0 mV	Channel 2 after Channel 1	50 mV/div	192 mV	2465 V	10 ns/div	10 ns

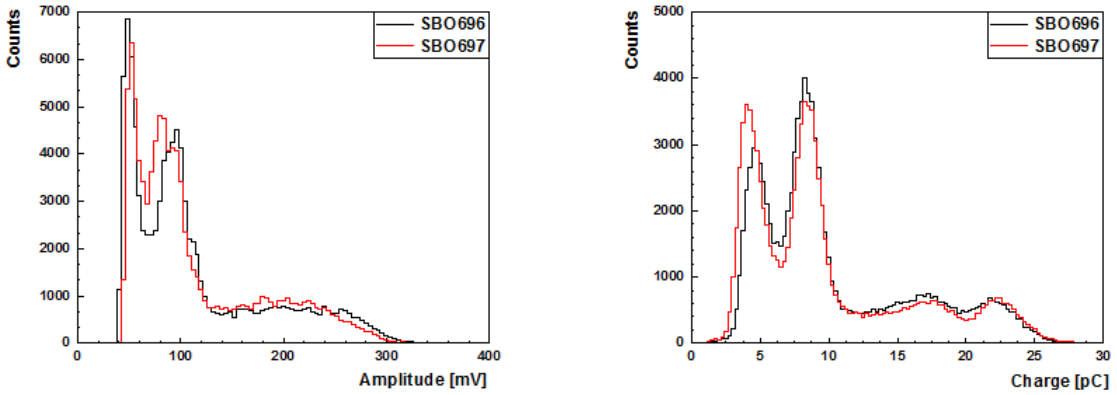

Fig. 2.11. Distribution of amplitude (a) and charge (b) of signals for 511 threshold calibration. Results obtained for different detectors are shown with different colors as indicated in the legend.

Having collected 100 000 events, charge and amplitude of every signal was calculated, and their distributions are shown in Fig. 2.11. Further on, the time difference distribution was determined for events for which both signals have charges in the range from 6 to 10 pC. The time at a given software threshold was calculated as a time at which the line fitted to the leading edge of the signal is crossing this threshold. Exemplary time difference spectrum is shown in Fig. 2.12. Such spectra have been determined for thresholds in the range from -50 mV to -10 mV. Fig. 2.13 shows dependence of the achieved time resolution as a function of the applied threshold. As a measure of the time resolution, a "sigma" parameter of the Gauss function fitted to the time diffrence spectra was used. It turned out that the best threshold to calculate time for signals coming from annihilation is equal to -17 mV.

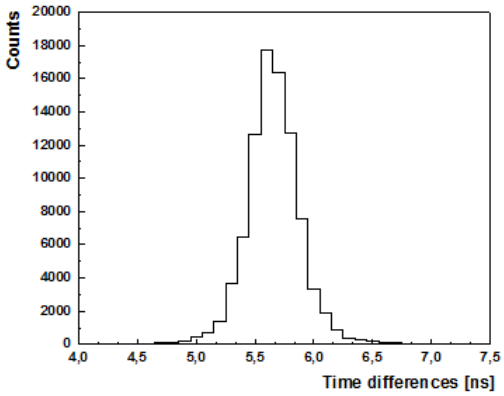

Fig. 2.12. Time differences between signals from two detectors. Only signals with charge ranging from 6 to 10 pC were taken into account. A time was calculated as a crossing of the line fitted to the leading edge at a value of -30 mV

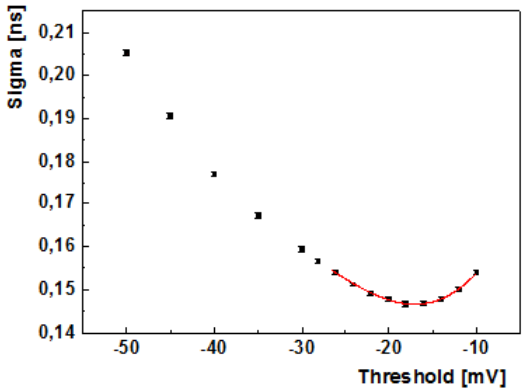

Fig. 2.13. Time resolution (sigma) as a function of the applied software threshold. Sigma denotes the fit to the spectrum of time differences between two 511 keV gamma quanta. A red line, plotted to guide the eye, indicates fitted polynomial model to the squares, which are results from calculations.

First step led to finding the best threshold for collecting gamma quanta from annihilation, so to complete optimization the best threshold for collecting „1274-511" events, had to be found. Measurement with high trigger on one detector was carried out with settings shown in Tab. 2.6. Results from this measurement are shown in Fig. 2.10. The time of the signal from annihilation quantum was calculated at the software threshold of -17 mV and the software threshold for the calculation of time of signals from deexcitation quanta was varied in the range from -120 mV to -10 mV. In the analysis it was required that the charge of signals from deexcitation quantum is larger than 18 pC. Fig. 2.14 illustrates time resolution as a function of the software threshold used for calculation of time of deexcitation gamma quanta. The best threshold for signals coming from deexcitation is around -27 mV.

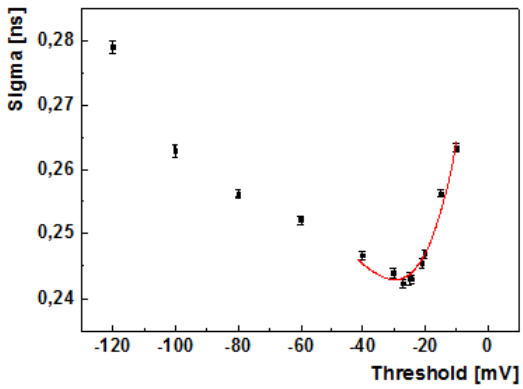

Fig. 2.14. Time resolution of the difference between signals from 511 keV and 1274 keV quanta as a function of the software threshold applied for determination of the time of signals from 1274 keV gamma quanta. The software threshold for calculation of the time from 511 keV was fixed to -17 mV. A red line, plotted to guide the eye, indicates fitted polynomial model to the squares, which are results from calculations.

From now one time difference (t_{diff}) between signal coming from deexcitation (1274 keV) and annihilation (511 keV) will be calculated as:

$$t_{diff} = t^{511}_{-17} - t^{1274}_{-27} \tag{2.12}$$

Chapter 3

Simulations

Simulations are useful if it is too difficult to optimize setup by making a lot of time consuming measurements. It will be shown here that, thanks to simulation of measurements, setup could be optimized much quicker than by doing it experimentally. With simulation model ready, one can simulate more complicate measurements in the future.

3.1 Simulated measurement

Simulations of the measurement enabled to study a ratio of the number of „511-511" events to the number of „1274-511" events as a function of the position of the radioactive source with respect to the detectors. Experimental setup is shown in Fig. 2.1a and settings from this measurements are given in Tab. 3.1.

Table 3.1: Settings with measurements with different shifts

Trigger	**Coincidence**	**Scale**	**Offset**	**Voltage on detectors**	**Timescale**	**Delay**
Settings for channel 1						
-22.0 mV	Channel 2 after Channel 1	40 mV/div	152 mV	2335 V	10 ns/div	8.2 ns
Settings for channel 2						
-22.0 mV	Channel 2 after Channel 1	40 mV/div	152 mV	2490 V	10 ns/div	8.2 ns

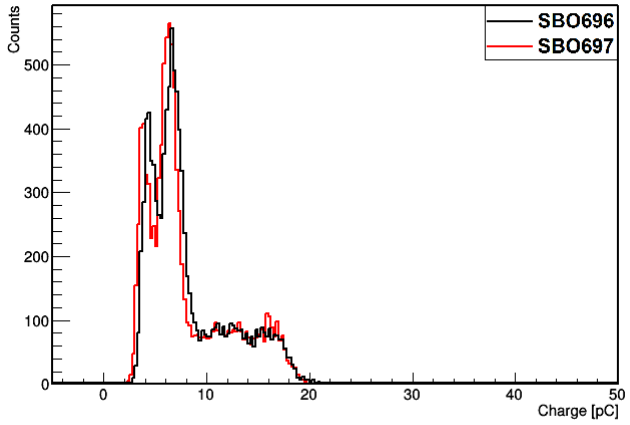

Fig. 3.1. Distribution of charges in measurement with shift Δ equal to 3 cm. Results obtained for different detectors are shown with different colors as indicated in the legend.

In order to validate the simulations a series of measurements were performed. Twenty thousand events were gathered for each of eight positions from $\Delta = 0$ to $\Delta = 4$ cm with a step of 0.5 cm. Fig. 3.1 shows that 10 pC is the boundary that separates 1274 keV from 511 keV. Therefore events „1274-511" are defined as these for which in one detector the signal charge is smaller than 9 pC and in the other the signal charge is larger than 10 pC. In turn „511-511" events are defined as these for which charge of signals in both detectors is smaller than 9 pC.

In real experiment even if Δ is larger than the radius of scintillation crystal, „511-511" events are still observed. This can happen due to the scattering of the gamma quanta in the detectors and due to the misidentification of the 1247 keV quantum as 511 keV quantum. Compton scattering of 1274 keV gamma in scintillation crystal might result in the energy deposition so low, that it is mismatched with the gamma quantum coming from annihilation, if charge of the signal is lower than 9 pC.

In order to simulate selection criteria it is necessary to determine (based on the experimental spectra) the following selection probabilities:
$P_{sel\,1274}$ - probability that the deexcitation quantum is classified as a deexcitation quantum (probability that the charge of the signal generated by the deexcitation quantum is larger than 10 pC);
$P_{sel\,511}$ - probability that annihilation quantum is classified as annihilation quantum (probability that the charge of the signal generated by the annihilation quantum is smaller than 9 pC and larger than the threshold);
$P_{1274\,mis\,511}$ - probability that deexcitation quantum is classified as annihilation quantum (probability that the charge of the signal generated by the deexcitation quantum is smaller than 9 pC and larger than the threshold).

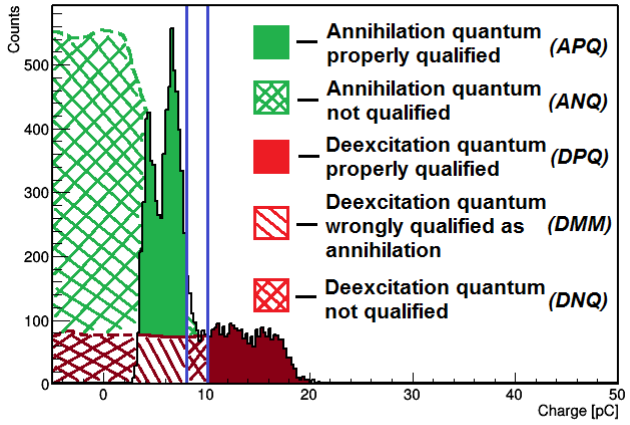

Fig. 3.2. Regions of deexcitation and annihilation quanta marked on distribution of charge measured with Δ equal to 3 cm. Results for SBO696 detector. Distribution, that is not seen in experiment because of the noise, is extrapolated and marked as dotted line. This distribution was measured separately using a TUCAN-8K. Blue lines indicate 9 pC and 10 pC used in the classification of events.

Considering charge spectrum shown in Fig. 3.2, one can estimate parameters for conditional probabilities:

$$P(sel\ 1274|1274\ absorbed) = \frac{DPQ}{DPQ + DMM + DNQ};$$

$$P(sel\ 511|511\ absorbed) = \frac{APQ}{ANQ + APQ};$$

$$P(1274\ mis\ 511|1274\ absorbed) = \frac{DMM}{DPQ + DMM + DNQ}.$$

To obtain parameters used in simulation one can use definition for total probability:

$$P_{sel\ 1274} = P(sel\ 1274|1274\ absorbed) \cdot P(1274\ absorbed) +$$

$$+P(sel\ 1274|1274\ not\ absorbed) \cdot P(1274\ not\ absorbed),$$

but $P(sel\ 1274|1274\ not\ absorbed) = 0$, so final form of selection probabilities will look as:

$$P_{sel1274} = P(sel\ 1274|1274\ absorbed) \cdot P(1274\ absorbed)$$

$$P_{sel\ 511} = P(sel\ 511|511\ absorbed) \cdot P(511\ absorbed)$$

$$P_{1274\ mis\ 511} = P(1274\ mis\ 511|1274\ absorbed) \cdot P(1274\ absorbed)$$

3.2 Simulation model

In model of simulated setup, radiation sensitive part is defined as a scintillation crystal BaF_2 7.1. Experimental setup is shown in Fig. 2.1b. Detectors were simulated as crystal

cylinders with radius of 1.9 cm and length of 3 cm. Simulation was performed to determine the efficiency of the registration of „511-511" and „1274-511" events as a function of the relative settings of detectors and the ^{22}Na source.

First assumption was, that in experiment there are only two types of radiation, with energy of 511 keV (annihilation) and 1274 keV (deexcitation) as in Fig. 1.2 and Fig. 1.3c, when both are emitted by the point-like source. The „511-511" event happens when signals in both detectors are qualified as signals originating from the 511 keV quanta. Condition for „1274-511" event is defined similarly.

Probability of absorption of gamma quantum with energy E on distance d from Lambert's Law is given by [23]:

$$\mathbb{P}\left(\text{Absorption of quantum with energy } E \text{ in distance } d\right) = 1 - \exp\left(-\mu_E \cdot d\right), \tag{3.1}$$

where μ_E is the linear absorption coefficient, which depends on the material and energy of gamma quantum. Values of coefficients for gamma quanta of 511 keV and 1274 keV passing through the BaF_2 crystal are as follows:[1]:

$$\begin{aligned} \mu_{511} &= 0.047 \tfrac{1}{cm}, \\ \mu_{1274} &= 0.017 \tfrac{1}{cm}. \end{aligned} \tag{3.2}$$

Simulations have been performed by Monte Carlo technique. Scheme of simulation process is described in Fig. 3.5. The angles needed for determination of gamma quanta direction were drawn from uniform distribution on sphere. Process of simulation is described below.

Iteration process started with assigning number of β^+ decay. Next two pairs of angles $\varphi_{1274}, \vartheta_{1274}$ and $\varphi_{511}, \vartheta_{511}$ were generated from uniform distribution on sphere for deexcitation (1274 keV) and annihilation (511 keV) quanta. Example of distribution of one million points simulated at a sphere is shown in Fig. 3.4. Angles φ, ϑ define unique direction $\vec{r}$ in spherical coordinate system, as shown pictorially in Fig. 3.3.

[1] http://www.crystals.saint-gobain.com/uploadedFiles/SG-Crystals/Documents/Technical/SGC%20Efficiency%20Calculations%20Brochure.pdf

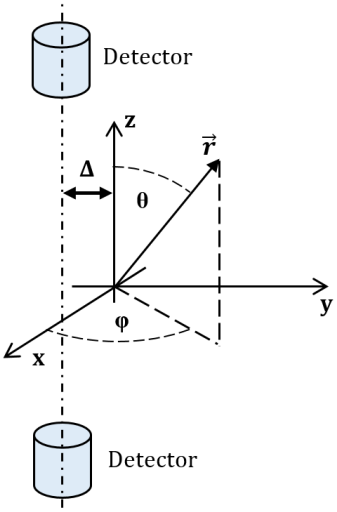

Fig. 3.3. Scheme of the simulated system. A ^{22}Na source emits gamma quanta from the origin of the coordinate system which is shifted by Δ with respect to the symmetry axis of the detectors.

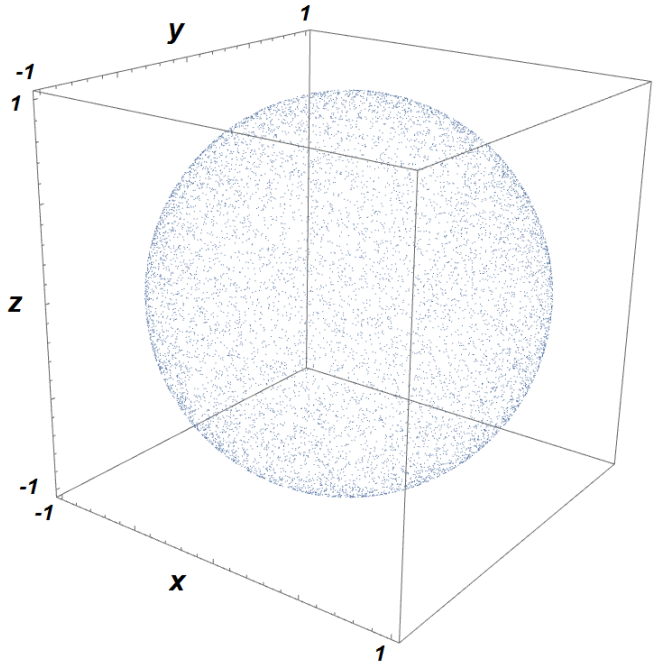

Fig. 3.4. Distribution of points with coordinates x, y, z, which were calculated from angles φ, ϑ, drawn from uniform distribution on sphere, for $r = 1$. Distribution obtained from one million draws.

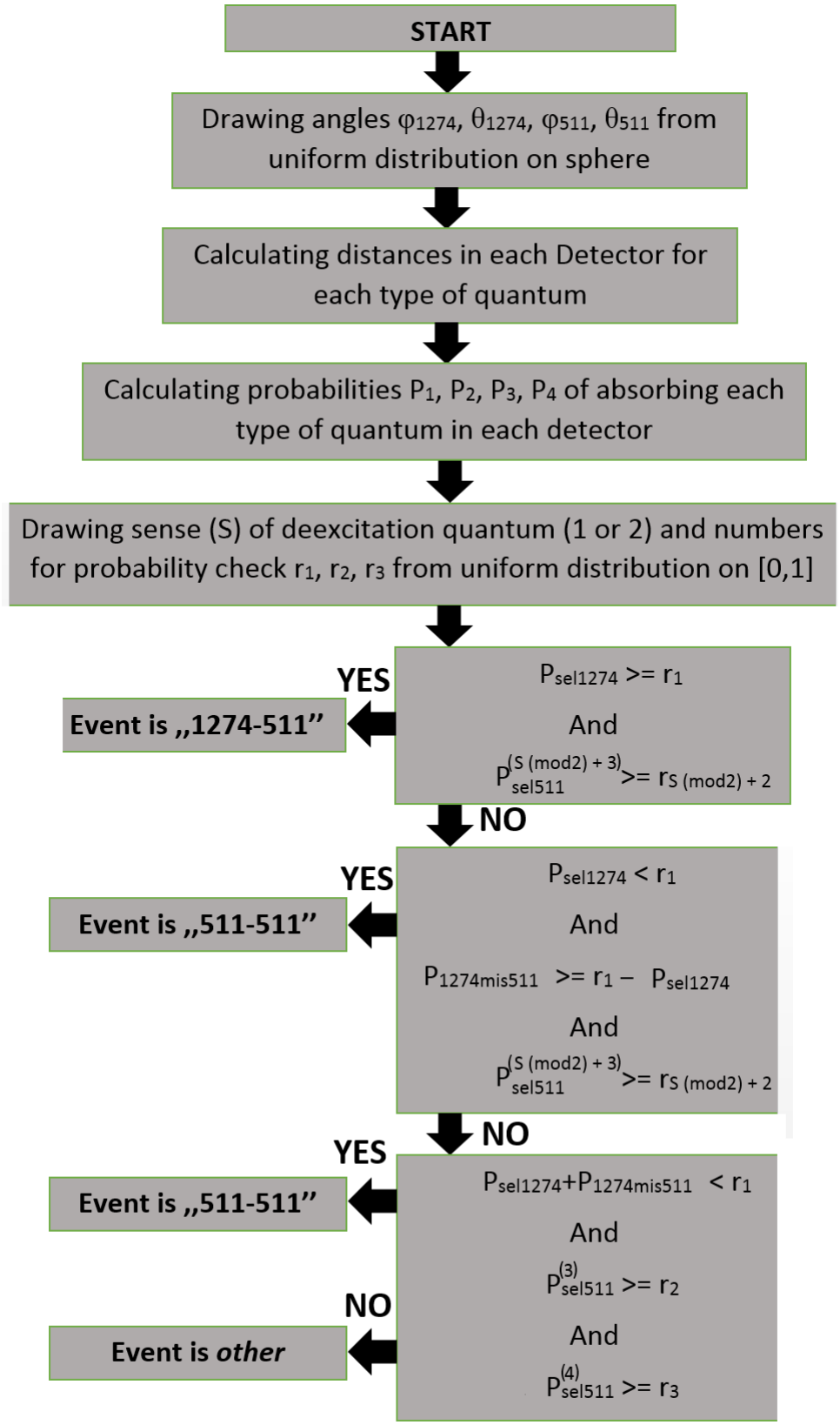

Fig. 3.5. Scheme of simulation process. Details are described in the text.

Having the directions of the gamma quanta propagation a next step is to calculate the length of the gamma quantum trajectory in the given detector. Calculations will be performed for angles φ, ϑ in general, as they can indicate pair of angles for annihilation or deexcitation quantum. For the source position at $\Delta = (x_0, y_0, z_0)$, the coordinates of a vector r pointing along the gamma quantum trajectory can be calculated as follows:

$$\begin{cases} x(r, \vartheta, \varphi) = r \cdot \sin\vartheta \cos\varphi + x_0 \\ y(r, \vartheta, \varphi) = r \cdot \sin\vartheta \sin\varphi + y_0 \\ z(r, \vartheta, \varphi) = r \cdot \cos\vartheta + z_0. \end{cases} \tag{3.3}$$

One can get z-axis coordinates, that solves:

$$x(z, \vartheta, \varphi)^2 + y(z, \vartheta, \varphi)^2 = R^2, \tag{3.4}$$

where R is radius of detector, and by using relation:

$$\begin{cases} x(z, \vartheta, \varphi) = (z - z_0) \cdot \cot\vartheta \cos\varphi + x_0 \\ y(z, \vartheta, \varphi) = (z - z_0) \cdot \cot\vartheta \sin\varphi + y_0. \end{cases} \tag{3.5}$$

Solving Eq. (3.4) will result in obtaining at most two z-axis coordinates, marked as z_1 and z_2 (in case of one solution $z_1 = z_2$) in real domain. These are the z coordinates of points where the gamma quanta leaves cylinder with radius R (including detector surfaces). In order to calculate a length of the gamma quanta trajectories inside the detectors (Det_{dist}) let us first define a detector (Det) as:

$$Det = \{(x, y, z) \in \mathbb{R} : x^2 + y^2 \leqslant R^2 \wedge z_d \leqslant z \leqslant z_b\}, \tag{3.6}$$

where $z_d \geqslant 0$ denotes z-coordinated of the detector edge closer to the source. The z coordinate of the second edge $z_b = z_d + L$, if L is the length of detector. The length of the gamma quantum trajectory in the detector Det_{dist} may be calculated as:

$$Det_{dist} = \begin{cases} 0 & z_1, z_2 \leqslant z_d \quad \text{or} \quad z_1, z_2 \geqslant z_b \\ d\left((x_d, y_d, z_d), (x_2, y_2, z_2)\right) & z_1 \leqslant z_d \quad \text{and} \quad z_d \geqslant z_2 \geqslant z_b \\ d\left((x_1, y_1, z_1), (x_b, y_b, z_b)\right) & z_2 \geqslant z_b \quad \text{and} \quad z_d \geqslant z_1 \geqslant z_b \\ d\left((x_d, y_d, z_d), (x_b, y_b, z_b)\right) & z_2 \geqslant z_b \quad \text{and} \quad z_1 \leqslant z_d, \end{cases} \tag{3.7}$$

where $d(X, Y)$ is euclidean distance and $x_i = x\left(z_i, \vartheta, \varphi\right)$, $y_i = y\left(z_i, \vartheta, \varphi\right)$ are given by Eq. (3.5) for $i \in \{1, 2, d, b\}$.

Second detector Det_2 will be defined by Eq. (3.8), and distances will be calculated similarly as in case of the first detector:

$$Det_2 = \{(x, y, z) \in \mathbb{R} : x^2 + y^2 \leqslant R^2 \wedge z_d^{(2)} \leqslant z \leqslant z_b^{(2)}\}, \tag{3.8}$$

where $z_d^{(2)} = -z_b$ and $z_b^{(2)} = -z_d$, what means that second detector is placed symmetrically with respect to the xy plane, to the first detector

As a next step probabilities of the interaction of the gamma quanta in the detectors are calculated. Probabilities are calculated from Eg. (3.1) for calculated distances. Conducting the above described procedure for deexcitation and annihilation quanta one will obtain probabilities:

$P^{(1)}_{1274}$, which is probability of absorbing 1274 keV quantum in first detector if direction of quantum is given by angles $\varphi_{1274}, \vartheta_{1274}$;
$P^{(2)}_{1274}$, which is probability of absorbing 1274 keV quantum in second detector if direction of quantum is given by angles $\varphi_{1274}, \vartheta_{1274}$;
$P^{(1)}_{511}$, which is probability of absorbing 511 keV quantum in first detector if direction of quantum is given by angles $\varphi_{511}, \vartheta_{511}$;
$P^{(2)}_{511}$, which is probability of absorbing 511 keV quantum in second detector if direction of quantum is given by angles $\varphi_{511}, \vartheta_{511}$.

Because in experiment there is only one deexcitation quantum, random number s was generated from $\{1, 2\}$ set, that will define unique sense (s) of this quantum (number of detector that quantum will aim for). If s is equal to 1, then quantum is aiming at first detector and probability of absorbing this 1274 keV quantum (P_{1274}) is equal to $P^{(1)}_{1274}$ and $P^{(2)}_{1274}$ is not taken under consideration. Otherwise $P_{1274} = P^{(2)}_{1274}$ and that probability is taken in further calculations.

Last step of the iteration is qualification of the simulated event to one of the three categories seen in experiment, „511-511", „1274-511", and *other*. Three random numbers (r_1, r_2, r_3) were generated from uniform distribution on interval $[0, 1]$ to check if event will take place. Next a simulated event is qualified as:

„1274-511"

if deexcitation quantum and at least one annihilation quantum were registered and properly classified:

$$P_{sel\ 1274} \geq r_1 \text{ and } P^{(s(\mathrm{mod}\ 2)+1)}_{sel\ 511} \geq r_{s(\mathrm{mod}\ 2)+2},$$

where (mod 2) is the modulo 2 operator, and $s(\mathrm{mod}\ 2) + 1$ indicates the number of detector which was not hit by 1274 keV quantum.
The event was qualified as:

„511-511"

if deexcitation quantum was qualified as annihilation quantum, and at least one annihilation quantum was registered and classified as annihilation:

$$P_{sel\ 1274} < r_1 \text{ and } P_{1274\ mis\ 511} \geq r_1 - P_{sel\ 1274}$$
$$\text{and } P^{(s(\mathrm{mod}\ 2)+1)}_{sel\ 511} \geq r_{s(\mathrm{mod}\ 2)+2}$$

or both annihilation quanta were registered but deexcitation was not

$$P_{sel\ 1274} + P_{1274\ mis\ 511} < r_1 \text{ and } P^{(1)}_{sel\ 511} \geq r_2 \text{ and } P^{(2)}_{sel\ 511} \geq r_3.$$

Finally the event was qualified as:

other

if event is classified neither as **„1274-511"** nor as **„511-511"**.

After m iterations, probability of registering „511-511" event is estimated as:

$$\mathbb{P}\,(\text{„511-511" event}) = \frac{N_{AA}}{m}, \tag{3.9}$$

where N_{AA} is number of iteration where „511-511" event was identified, and m denotes number of all simulated events. After similar procedure probability of registering „1274-511" event is estimated as:

$$\mathbb{P}\,(\text{„1274-511" event}) = \frac{N_{AE}}{m}, \tag{3.10}$$

where N_{AE} is number of iteration where „1274-511" event was identified after m iterations.

3.3 Comparison with measurement

Final results of simulations compared with results from measurement are shown in Fig. 3.6. It can be seen that measurement results are consistent with the simulation within error bars.

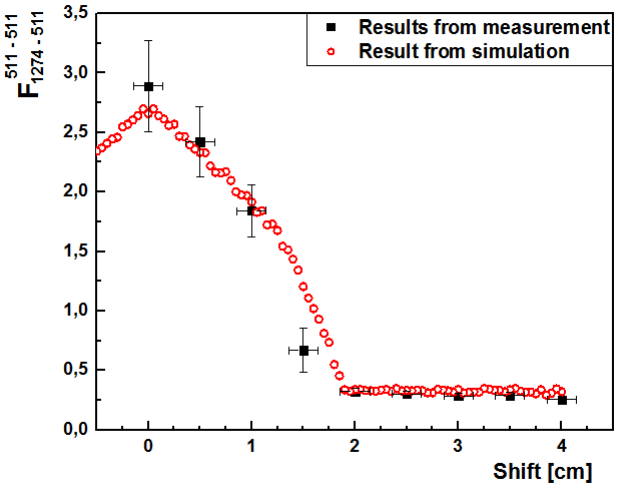

Fig. 3.6. Ratio of number of „511-511" events to the number of „1274-511" events as a function of the shift (Δ) of the source with respect to the detector axis. Comparison of results from simulations (red circles) and result from measurement (black squares)

Simulations helped finding optimal (Δ) value that would maximize number of „1274-511" events compared to number of „511-511". This shift (Δ) should be greater or equal than 2 cm, what agrees with predictions from calibration process. Greater number of collected events in measurement and better estimation of probabilities of selection ($P_{sel\ 1274}$, $P_{sel\ 511}$, $P_{1274\ mis\ 511}$) should improve measurement accuracy and its consistency with simulation.

Chapter 4

Analysis procedure for PALS

Last thing after assembling and calibrating PALS apparatus is to find a way to analyze PALS spectra, which are gathered as histograms of time differences, between signals from two detectors. There is no simple method for fitting these spectra. Here an iterative procedure will be proposed, for getting distribution of ortho-positronium lifetimes in material, from which one can obtain free volumes radius distribution, with ready models given for example by Tao-Eldrup, Eq. (1.1).

4.1 Discrete size distribution of free volumes

First step of analysis is to get the expression for decay time, when material has discrete size distribution of free volumes, what shall manifest itself in discrete distribution of positronium lifetimes. Lifetime of ortho-positronium (τ) in free volume depends on its radius (R). For a given radius R an ortho-positronium life-time distribution is expressed as:

$$E(t;\tau) = \frac{1}{\tau(R)} \exp\left(-\frac{t}{\tau(R)}\right). \tag{4.1}$$

The experimental resolution of the time measurement may be approximated by the Gauss distribution as:

$$G(t;t_0,\sigma) = \frac{1}{\sqrt{2\pi}\cdot\sigma} \exp\left(-\frac{(t-t_0)^2}{2\cdot\sigma^2}\right), \tag{4.2}$$

where t_0 denotes a time offset of the detector due to e.g. the differences in signal cables lengths, and different thresholds for time calculations. Resolution of the apparatus (Res) is often expressed in terms of full width of half maximum (FWHM) which can be calculated from the σ parameter as:

$$Res = 2\sqrt{2\ln 2}\cdot\sigma. \tag{4.3}$$

The measured time distribution ($F(t)$) of the lifetime of ortho-positronium atoms in free volumes of size R may be approximated by the one-sided convolution of functions E and G defined in eq. (4.1) and (4.2):

$$F(t) = (E * G)(t) \stackrel{df}{=} \int_0^t E(x;\tau)\cdot G(t-x;t_0,\sigma)dx \tag{4.4}$$

$$\int_0^t E(x;\tau)\cdot G(t-x;t_0,\sigma)dx = \frac{1}{\sqrt{2\pi}\cdot\sigma\tau}\int_0^t \exp\left(-\frac{x}{\tau}-\frac{(t-x-t_0)^2}{2\cdot\sigma^2}\right)dx = \dots$$

Expression under integral could be transformed into part dependent on x, and the rest, what will simplify further calculations:

$$\exp\left(-\frac{\mathbf{x}}{\tau}-\frac{(t-\mathbf{x}-t_0)^2}{2\cdot\sigma^2}\right) = \exp\left(\frac{\sigma^2}{2\cdot\tau^2}-\frac{t-t_0}{\tau}\right)\exp\left(-\frac{\left(t-\mathbf{x}-t_0-\frac{\sigma^2}{\tau}\right)^2}{2\cdot\sigma^2}\right). \quad (4.5)$$

Moreover also useful would be substitution given by:

$$p = \frac{t-x-t_0-\frac{\sigma^2}{\tau}}{\sqrt{2}\cdot\sigma} \qquad \rightarrow \qquad dp = -\frac{dx}{\sqrt{2}\cdot\sigma}. \quad (4.6)$$

which leads to following expression:

$$\dots \overset{(4.5)(4.6)}{=} \frac{1}{\sqrt{\pi}\tau}\exp\left(\frac{\sigma^2}{2\cdot\tau^2}-\frac{t-t_0}{\tau}\right)\int_{\frac{-t_0-\frac{\sigma^2}{\tau}}{\sqrt{2}\cdot\sigma}}^{\frac{t-t_0-\frac{\sigma^2}{\tau}}{\sqrt{2}\cdot\sigma}}\exp\left(-p^2\right)dp = \dots$$

Further on using error function:

$$\mathrm{erf}(x) \overset{df}{=} \frac{2}{\sqrt{\pi}}\int_0^x \exp\left(-s^2\right)ds, \quad (4.7)$$

and expressing $F(t)$ as:

$$F(t) = \dots = \frac{1}{\sqrt{\pi}\tau}\exp\left(\frac{\sigma^2}{2\cdot\tau^2}-\frac{t-t_0}{\tau}\right)\left(\int_0^{\frac{t-t_0-\frac{\sigma^2}{\tau}}{\sqrt{2}\cdot\sigma}}\exp\left(-p^2\right)dp + \int_{\frac{-t_0-\frac{\sigma^2}{\tau}}{\sqrt{2}\cdot\sigma}}^0\exp\left(-p^2\right)dp\right),$$

one obtains a following formula approximating the experimental lifetime distributions of ortho-positronium in free volumes with radius R and a mean lifetime τ:

$$F(t;\tau,t_0,\sigma) \overset{(4.7)}{=} \frac{1}{2\cdot\tau}\exp\left(\frac{\sigma^2}{2\cdot\tau^2}-\frac{t-t_0}{\tau}\right)\left(\mathrm{erf}\left(\frac{t-t_0-\frac{\sigma^2}{\tau}}{\sqrt{2}\cdot\sigma}\right)-\mathrm{erf}\left(\frac{-t_0-\frac{\sigma^2}{\tau}}{\sqrt{2}\cdot\sigma}\right)\right) \quad (4.8)$$

Error function is well known, and despite that there are no analytic form of this function, its tabularized with good accuracy. Use of tabularized values of error function shortens computing time, when fitting formula to the experimental distribution.

4.2 Fitting of discrete mean-lifetime distributions

Fitting formula in discrete situation will use assumption, that material has a discrete distribution of free volume radius, what will lead to discrete ortho-positronium mean lifetime distributions:

$$f(t) = y_0 + \sum_{i=1}^{n_\tau} I_i \cdot F\left(t;\tau_i,t_0,\sigma\right), \quad (4.9)$$

where t is time differences between signals registered by detectors , y_0 denote the background level, and n_τ is the number of main components, usually less than 10. I_i and τ_i denote intensity and mean lifetime of i-th component, respectively. $F(t;\tau,t_0,\sigma)$ defined by Eq. (4.8) denotes time distribution for i-th component. Finally, σ and t_0 denote experimental resolution and time offset defined in the previous section.

In more general case, when the time resolution of the detection system is described by the sum of Gauss functions, then a fitted formula is expressed as:

$$f(t) = y_0 + \sum_{i=1}^{n_\tau} \sum_{j=1}^{n_{Gauss}} I_i \cdot \alpha_j \cdot F\left(t;\tau_i,t_0^{(j)},\sigma_j\right), \tag{4.10}$$

where α_j is the fraction of given Gauss distribution and $\sum_{j=1}^{n_{Gauss}} \alpha_j = 1$.

Levenberg-Marquardt algorithm in ROOT program, will be used to fit formula (4.10) to collected time difference histogram.

4.3 Fitting of continuous mean-lifetime distributions

In reality, sizes of pores in the material and hence the mean-lifetimes of positronium atoms are distributed continuously. Therefore, the derivations of the formulas from the previous section need to be extended from the discrete to the continuous mean lifetime distribution. It will be assumed that the distribution of the mean lifetimes of ortho-positronium atoms, may be approximated by a sum of Gauss functions. For a single Gauss function one may express the lifetime distribution by convoluting formula from Eq. (4.4) with another Gauss function $G(\tau)$ describing the distribution of mean lifetimes:

$$\left(E(t,\tau) * G(t) * G(\tau)\right)(t,\tau) \stackrel{df}{=} \int_0^\tau \int_0^t E(x;y) \cdot G(t-x;t_0,\sigma) \cdot G(\tau-y;\tau,\rho)dxdy. \tag{4.11}$$

Eq. (4.11) cannot be expressed in the simple form, as derived for the discrete case (Eq. (4.8)). Therefore, in order to accelerate a fitting procedure instead of Eq. (4.11) procedure will be as follows: First Eq. (4.10) is fitted to the histogram with n_τ in the range from 2 to 6. This allows to estimate a detector parameters as σ and t_0.
Next a grid of lifetimes is defined with
the interval of 5 ps for 10 ps $\leq \tau <$ 1 ns;
the interval of 10ps for 1 ns $\leq \tau <$ 10 ns;
and interval of 100 ps for 10 ns $\leq \tau <$ 142 ns.
And as last step a fitting of formula (4.10) is done with fixed detector parameters σ and t_0 and for fixed times from the above defined grid. Thus the only varying parameters are intensities of mean lifetimes from the grid. Whole idea is shown in Fig. 4.1.

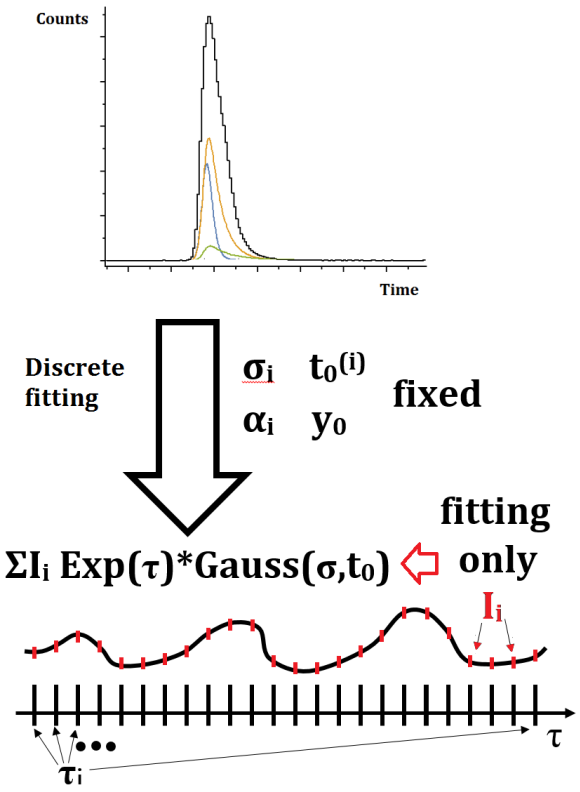

Fig. 4.1. Obtaining grid of lifetimes using iterative procedure. Part of parameters from discrete fit is fixed and transferred into continuous fitting.

Having grid of lifetimes, also Levenberg-Marquardt algorithm is used to fit all I_i and to get distribution of mean lifetimes, from which one can get distribution of free volume radius using proper transformation.

Chapter 5

Example PALS measurements

Materials chosen to tests were Silicon (Si), and Polyvinyl toluene (PVT). These materials were chosen because in Si the ortho-positronium is not created and in PVT the distribution of mean lifetime of ortho-positronium is well known. In semiconductors like Si, which is densely packed (diamond lattice), with high electron density it is unlikely that ortho-positronium will be created. All measurement were performed in room temperature, in air.

5.1 Measurement with silicon plates

Silicon was in form of two plates, with (111) plane exposed. ^{22}Na isotope source was covered in the thin Kapton foils in order to minimize the positron absorption [11], [9]. Si plates were placed around the source, (111) plane polished towards source. Setup for measurement conducted with Si plates is shown in Fig. 5.1, and settings are given in Tab. 5.1.

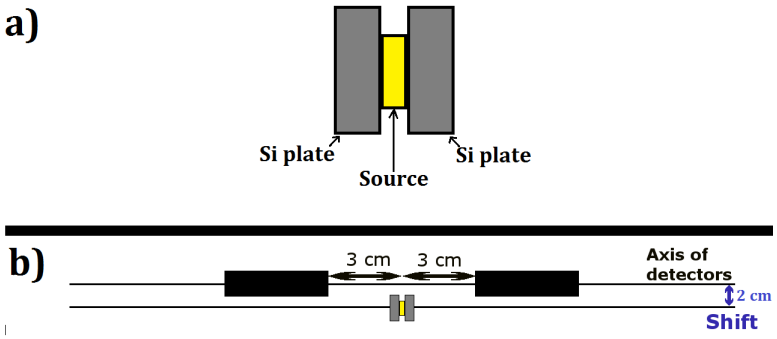

Fig. 5.1. (a) Scheme of silicon plates and ^{22}Na source. (b) Scheme of setup for silicon plates measurement.

Five hundred thousand events were collected. Charge spectra obtained for both detectors are shown in Fig. 5.2. „1274-511" events were classified requiring that charge of the signal from the SBO696 detector is larger than 14 pC and the charge of the signal from SBO697 is smaller than 9 pC. Distribution of time differences (defined in Eq. (2.12)) is shown in Fig. 5.3.

Table 5.1: Settings for measurement with Si plates

Trigger	Coincidence	Scale	Offset	Voltage on detectors	Timescale	Delay
Settings for channel 1 (SBO696)						
-110.0 mV	Channel 2 after Channel 1	50 mV/div	192 mV	2300 V	20 ns/div	40 ns
Settings for channel 2 (SBO697)						
-25.0 mV	Channel 2 after Channel 1	20 mV/div	78 mV	2465 V	20 ns/div	40 ns

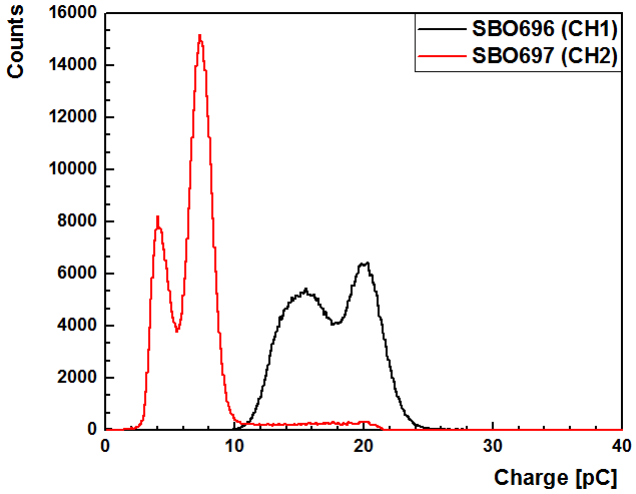

Fig. 5.2. Charge spectrum from Si plates measurement. Results obtained for different detectors are shown with different colors as indicated in the legend.

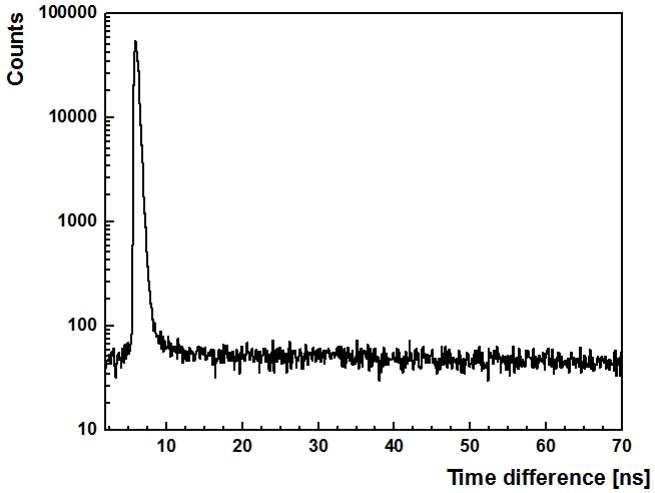

Fig. 5.3. Histogram of time differences between channel 1 and channel 2, from Si plates measurement.

Table 5.2: Fit parameters from Si plates measurement

Parameter	Value	Units
y_0	7.835 (91)	-
I_1	9.99 (07)	%
I_2	90.11 (07)	%
tau_1	0.370 (06)	ns
tau_2	0.216 (11)	ns
α_1	56.9 (1.4)	%
$t_0^{(1)}$	5.74 (04)	ns
$t_0^{(2)}$	6.16 (07)	ns
σ_1	0.101 (09)	ns
σ_2	0.179 (09)	ns
χ^2	446.02	

Having time difference histogram, fitting procedure was ready to start. Formula that was fitted contained sum of two Gaussian distribution with parameters $(\alpha_1, t_0^{(1)}, \sigma_1)$ and $(\alpha_2, t_0^{(2)}, \sigma_2)$. Results from fitting are shown in Fig. 5.4. One can see that there are two mean lifetime component. First amounting to 370 ns is coming from free positron annihilation in Kapton foil with intensity 9.99% [11]. Second component with lifetime of 0.218 ns is coming from free positron annihilation in silicone. The obtained values agree with the results known from literature [24].
Final distribution of mean lifetimes show large dispersion of fitted components. This is probably caused by impurities in silicon plates. Annealing of plates before measurement should improve resolution on lifetime grid. Better statistic of the measurement or measurements in vacuum should bring better estimation of apparatus parameters in discrete situation, what also should improve results of the fitting.

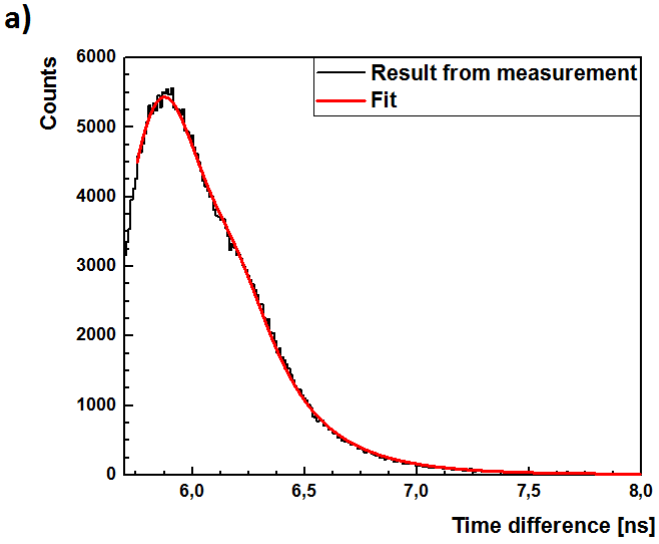

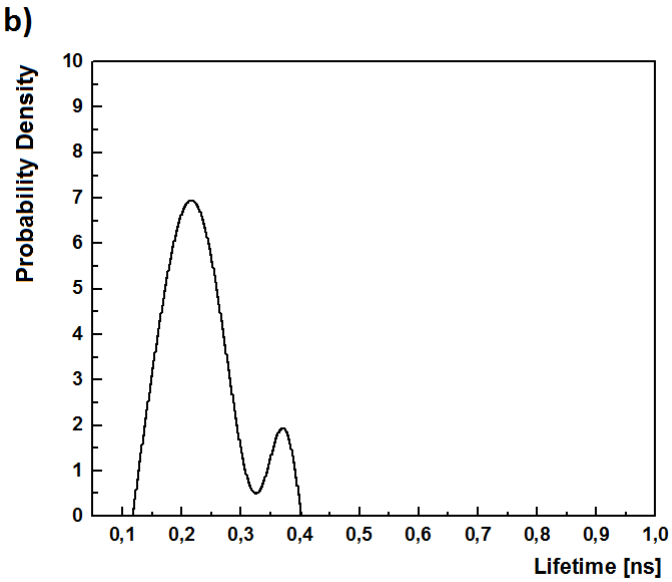

Fig. 5.4. (a) Time difference spectrum from silicon plates measurement with fitted model, indicated as red line.
(b) Distribution of mean lifetimes obtained from fitting silicon plates time difference spectrum. Distribution is normalized to 1.

This measurement helped to estimate fraction and lifetime of positron annihilation in source material - Kapton foil. This estimation will be used in studies of other materials.

5.2 Measurement with polyvinyl toluene

Next material chosen for test measurements was Polyvinyl toluene. Polyvinyl toulene was obtained using a method described in reference [5], in cylinder form. This material should show some long-lived component of ortho-positronium, because of existence of free volumes between polymer chains. ^{22}Na source in Kapton foil was used, setup is shown in Fig. 5.5 and settings are given in Tab. 5.3.

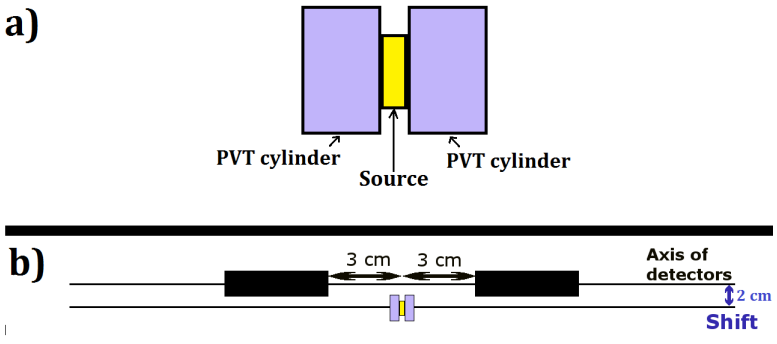

Fig. 5.5. (a) Scheme of polyvinyl toluene and ^{22}Na source.
(b) Scheme of setup for PVT measurement.

Table 5.3: Settings for measurement of polyvinyl toulene

Trigger	Coincidence	Scale	Offset	Voltage on detectors	Timescale	Delay
Settings for channel 1 (SBO696)						
-110.0 mV	Channel 2 after Channel 1	50 mV/div	192 mV	2300 V	20 ns/div	40 ns
Settings for channel 2 (SBO697)						
-25.0 mV	Channel 2 after Channel 1	20 mV/div	78 mV	2465 V	20 ns/div	40 ns

As in Si plates measurement, five hundred thousand events were collected. Charge spectra obtained for both detectors are shown in Fig. 5.6. „1274-511" events were classified requiring that charge of the signal from the SBO696 detector is larger than 15 pC and the charge of the signal from SBO697 is smaller than 10 pC. Difference in classification, compared to previous measurement is due to temperature dependence of BaF_2 detectors gain. Distribution of time differences (defined in Eq. (2.12)) is shown in Fig. 5.7.

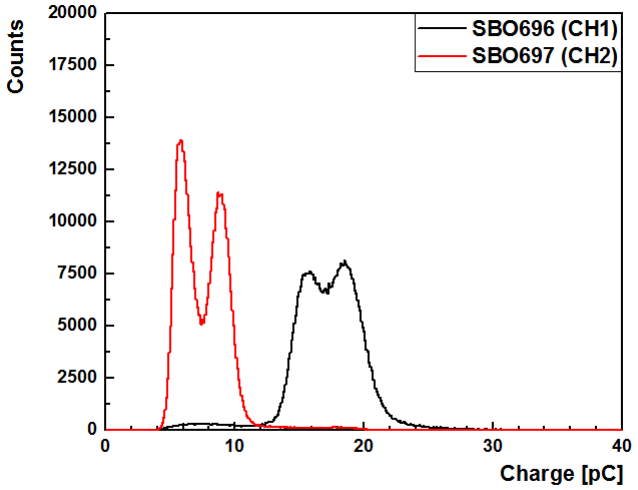

Fig. 5.6. Charge spectrum from polyvinyl toluene measurement. Results obtained for different detectors are shown with different colors as indicated in the legend.

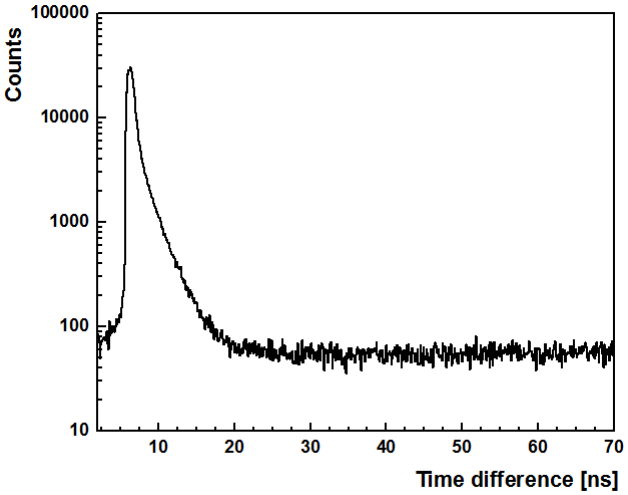

Fig. 5.7. Histogram of time differences between channel 1 and channel 2, from polyvinyl toluene measurement.

Fitting procedure was launched. Results are shown in Tab. 5.4. One can see, besides lifetime components coming from free positrons annihilation in Kapton foil ($\tau_3 = 0.37$ ns), a components coming from annihilation of ortho-positronium ($\tau_4 = 0.53$ ns, $\tau_5 = 1.9$ ns, $\tau_6 = 2.9$ ns) and annihilation of para-positronium ($\tau_1 = 0.127$ ns) in polymer.

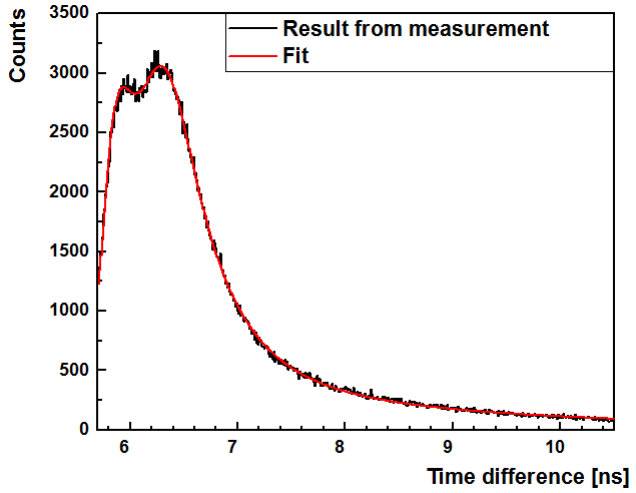

Fig. 5.8. Time difference spectrum from polyvinyl toluene measurement with fitted model, indicated as red line.

Lifetime τ_1 agrees with values coming from literature (0.125 ns [11]) in the limits of uncertainties. Second component ($\tau_2 = 0.29$ ns) probably is coming from annihilation of free positrons in PVT, which in literature varies from 200 to 300 ps [25]. Longer lifetimes τ_5, τ_6 coming from annihilation of o-Ps in free volumes are close to the values for polymers (PTFE, PE [12], PMMA [26]) with similiar structure. Better statistics, same as in previous measurement, should improve obtained mean lifetime distributions quality.

Table 5.4: Fit parameters from PVT measurement

Parameter	**Value**	**Units**
y_0	13.25 (15)	-
I_1	2.17 (35)	%
I_2	0.76 (01)	%
I_3	9.14 (02)	%
I_4	1.64 (02)	%
I_5	62.89 (66)	%
I_6	23.39 (36)	%
tau_1	0.127 (02)	ns
tau_2	0.294 (07)	ns
tau_3	0.375 (05)	ns
tau_4	0.531 (09)	ns
tau_5	1.90 (12)	ns
tau_6	2.91 (10)	ns
α_1	52.5 (1.2)	%
$t_0^{(1)}$	5.754 (03)	ns
$t_0^{(2)}$	6.176 (04)	ns
σ_1	0.107 (05)	ns
σ_2	0.183 (04)	ns
χ^2	518.62	

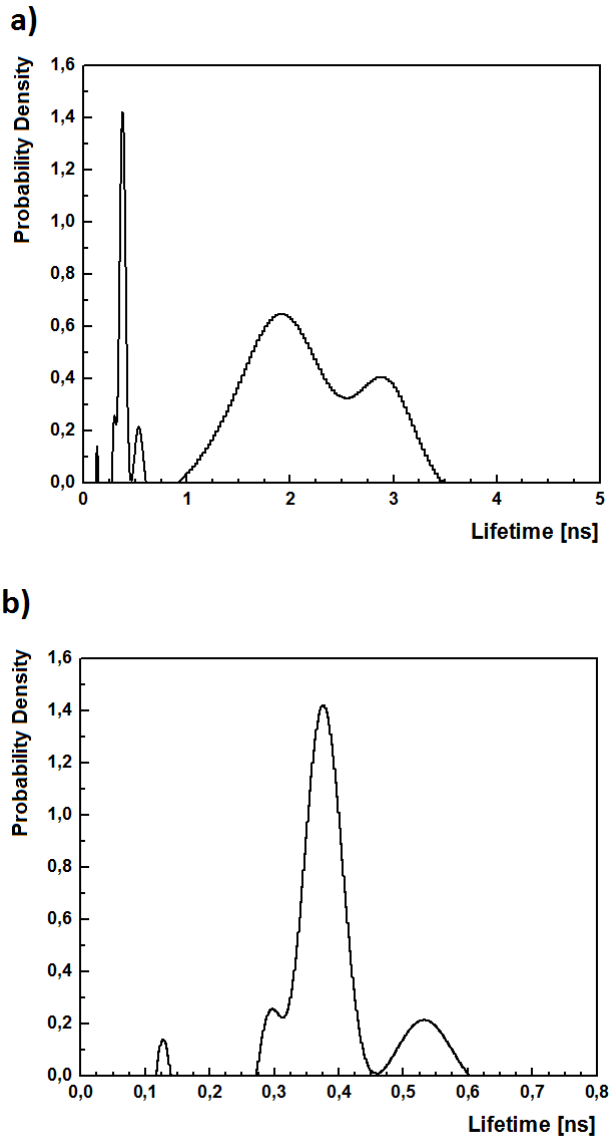

Fig. 5.9. Distribution of mean lifetimes in polyvinyl toluene (a) in full range (b) for short lifetimes. Distributions are normalized to 1.

Fourth component with mean lifetime $\tau_4 = 0.53$ ns can be derived from ortho-positronium annihliation in defects or inpurities on surface of PVT cylinders, because of its low intensity and appearing of similar component in previous polymer studies (PTFE, PE [12], PMMA [26]). Components coming from ortho-positronium, beside fourth component with unknown source, allows to calculate distribution of free volume radius in polyvinyl toluene. Free volumes radius will be estimated from Tao-Eldrup model, given in Eg. (1.1). Resulting radius distribution is shown in Fig. 5.10.

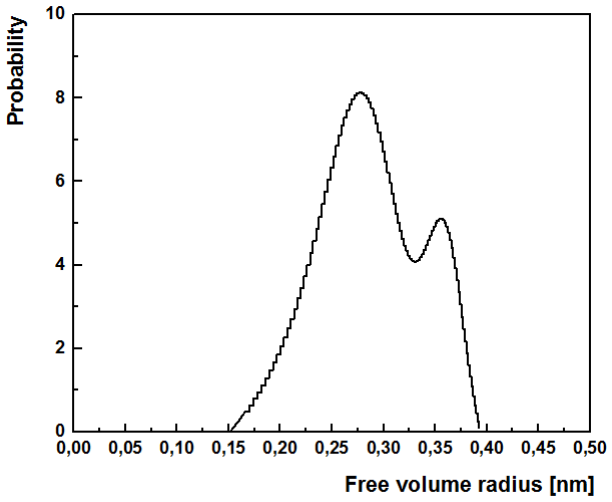

Fig. 5.10. Distribution of free volume radius in polyvinyl toluene, calculated using Tao-Eldrup formula, Eq. (1.1).

Chapter 6

Conclusions and summary

PALS setup was assembled using two BaF_2 detectors. Signals were gathered by oscilloscope, and analyzed individually for given event. Setup was optimized for use in PALS measurements. Both detectors gains were equalized. First detector (SBO696) was assigned to collect deexcitation quanta, when the second one (SBO697) was collecting annihilation quanta to maximize collection of „1274-511" events.

PALS measurement procedure was successfully simulated. Simulations allowed to additionally optimize the setup, by finding the best source position in relation to detectors, without doing time consuming measurements. Results from simulations agree with results from real measurement, in the limits of uncertainties. Thanks to simulations optimal shift (Δ) of the source position was found. Shift that maximizes collection of „1274-511" events, should be at least 2 cm.

Optimal thresholds for each type of gamma quantum in time calculations were determined, by minimizing deviation of calculated times.

Fitting formula for PALS spectrum was elaborated, as a convolution of the exponential decay, describing o-Ps annihilation, and Gauss distribution that represented apparatus time resolution. The derived formula was adapted for fitting of PALS spectra in the general case of the continuous mean lifetime distributions.

Having setup and analysis procedure ready, measurement for two samples were done. First sample was silicon plates used in production of solar cells, with plane (111) exposed. Results from PALS measurement showed, that there are two lifetimes components, one coming from annihilation in Kapton foil (0.370 ns), and other coming from annihilation in Si (0.218 ns). That is expected, as Si lattices is diamond-like, with high electron density in the lattice, what decreases probability of forming positronium.

Second sample was polyvinyl toluene, which was example of material where positronium can be trapped in its free volumes. Result from measurement showed existence of long-lived component from annihilation in PVT with lifetime of 1.9 ns and 2.91 ns, what transfers to free

volumes sizes with around 0.277 nm and 0.356 nm, by using Tao-Eldrup formula Eq. (1.1). This agrees with literature values of similar materials.

Measurements of the samples proved that apparatus assembled for PALS works properly and accurate. These results agrees with prediction and literature. Fitting procedure is working acceptably, what is good prognostic for the future experimentation with the J-PET detector.

Bibliography

[1] *Test of a single module of the J-PET scanner based on plastic scintillators* P. Moskal et. al, Nuclear Instruments and Methods in Physics, Vol. 764, Pages 317 - 321 (2014)

[2] *J-PET analysis framework for the prototype TOF-PET detector* W. Krzemień et. al, Bio-Algorithms and Med-Systems, Vol. 10, Pages 33 – 36 (2014)

[3] *Compressive sensing of signals generated in plastic scintillators in a novel J-PET instrument* L. Raczyński, Nuclear Instruments and Methods in Physics, Vol. 786, Pages 105 - 112 (2015)

[4] *Hit time and hit position reconstruction in the J-PET detector based on a library of averaged model signals* P. Moskal et. al, Acta Physica Polonica A, Vol. 127, Pages 1495 - 1499 (2015)

[5] *A pilot study of the novel J-PET plastic scintillator with 2-(4-styrylphenyl)benzoxazole as a wavelength shifter* A. Wieczorek et. al, Acta Physica Polonica A, Vol. 127, Pages 1487 - 1490 (2015)

[6] *Multiple scattering and accidental coincidences in the J-PET detector simulated using GATE package* P. Kowalski, Acta Physica Polonica A, Vol. 127, Pages 1505 - 1512 (2015)

[7] *Time resolution of the plastic scintillator strips with matrix photomultiplier readout for J-PET tomograph* P. Moskal, Physics in Medicine and Biology, Vol. 61, Pages 2025 - 2047 (2016)

[8] *Calibration of photomultipliers gain used in the J-PET detector* T. Bednarski, Bio-Algorithms and Med-Systems, Vol. 10, Pages 13 - 17 (2014)

[9] *Potential of the J-Pet detector for studies of discrete symmetries in decays of positronium atom - a purely leptonic system* P. Moskal et. al, Acta Physica Polonica B, No. 2, Vol. 47, Pages 509 - 236 (2016)

[10] *A feasibility study of ortho-positronium decays measurement with the J-PET scanner based on plastic scintillators* D. Kamińska et. al, The European Physics Journal C, Vol. 76, Pages 445 - 459 (2016)

[11] *Determination of the 3γ fraction from positron annihilation in mesoporous materials for symmetry violation experiment with J-PET scanner* B. Jasińska et. al, Acta Physica Polonica B, No. 2, Vol. 47, Pages 453 - 460 (2016)

[12] *The Temperature Dependence of the Local Free Volume in Polyethylene and Polytetrafluoroethylene: A Positron Lifetime Study* G. Dlubek, Journal of Polymer Science: Part B: Polymer Physics, Vol. 36, Pages 1513 – 1528 (1998)

[13] *Single shot positron annihilation lifetime spectroscopy* D. B. Cassidy et. al, Applied Physics Letters, Vol. 88, 194105 (2006)

[14] http://www.soarnol.com/eng/solution/solution060313.html

[15] http://web-docs.gsi.de/ wolle/Schuelerlabor/

[16] *Can Tao-Eldrup Model Be Used at Short o-Ps Lifetime?*, B. Zgardzinska, Acta Physica Polonica A, No. 3, Vol. 125, Pages 700 - 701 (2014)

[17] *Pore structure of silica gel: A comparative study through BET and PALS* D. Dutta et. al, Chemical Physics 312, Pages 319 - 324 (2005)

[18] http://soft-matter.seas.harvard.edu/index.php/Insoluble_monolayers

[19] *Free-Volume and Crystallinity in Low Molecular Weight Poly(ethylene oxide)*, Jose C. Machado et. al, Journal of Polymer Science Part B: Polymer Physics, Vol. 45 Pages 2400 - 2409 (2007)

[20] *Mechanical properties and fracture toughness of organo-silicate glass (OSG) low-k dielectric thin films for microelectronic application*, J.Vella et. al, International Journal of Fracture Vol. 120(1) Pages 487 - 499 (2003)

[21] *Non-destructive characterisation of porous low-k dielectric films*, M. R. Baklanov, K.P. Mogilnikov, Microelectronic Engineering, Vol. 64, Pages 335 – 349 (2002)

[22] *Calibration of photomultipliers gain used in the J-PET detector*, T. Bednarski et.al, Bio-Algorithms and Med-Systems 10(1), Pages 13 – 17 (2014)

[23] *The Beer-Lambert Law* D. F. Swinehart, Journal of Chemistry Education, Vol. 39, Pages 333 - 335 (1962)

[24] *Positron line-shape parameters and lifetimes for semiconductors: Systematics and temperature effects* S. Dannefaer et. al, Physical Review B, No. 4, Vol. 55, Pages 2182 - 2188 (1997)

[25] *Positron irradiation effects in simple organic solids* R. Zaleski, Radiation Physics and Chemistry, Vol. 77, Pages 1306 – 1310 (2008)

[26] *On the Measurement of Structural Relaxation in Polymers Using Positron Annihilation lifetime Spectroscopy* X. S. Li et. al, Journal of Polymer Science: Part B Polymer Physics, Vol. 31, Pages 869 - 873 (1993)

Chapter 7

Supplements

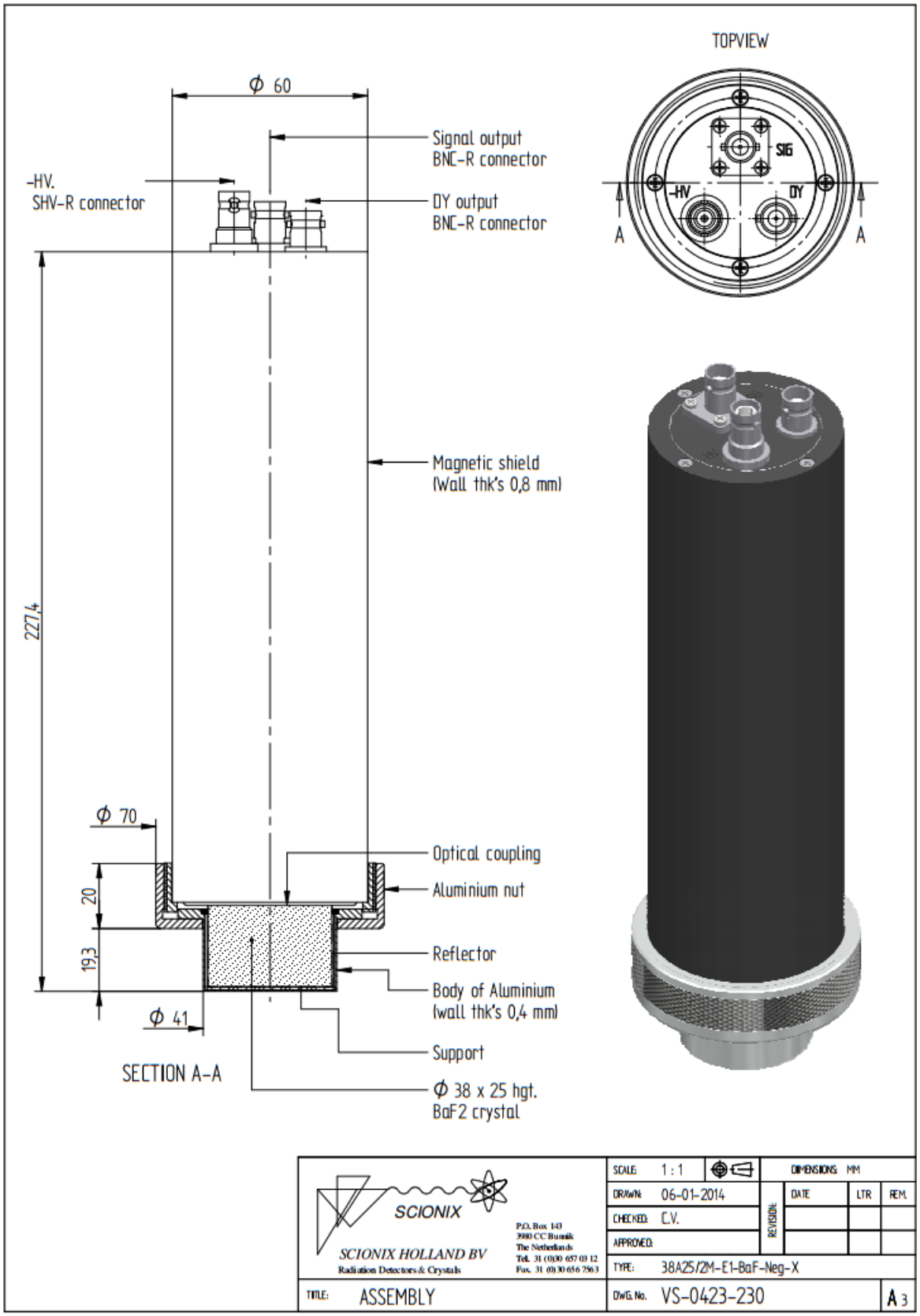

Figure 7.1: Scheme of BaF_2 detectors used to assembly PALS setup.